



# Raman spectroscopic techniques for detecting structure and quality of frozen foods: principles and applications

Wenyang Zhang , Ji Ma & Da-Wen Sun

To cite this article: Wenyang Zhang , Ji Ma & Da-Wen Sun (2020): Raman spectroscopic techniques for detecting structure and quality of frozen foods: principles and applications, Critical Reviews in Food Science and Nutrition, DOI: [10.1080/10408398.2020.1828814](https://doi.org/10.1080/10408398.2020.1828814)

To link to this article: <https://doi.org/10.1080/10408398.2020.1828814>



Published online: 09 Oct 2020.



Submit your article to this journal [↗](#)



View related articles [↗](#)



View Crossmark data [↗](#)

REVIEW



# Raman spectroscopic techniques for detecting structure and quality of frozen foods: principles and applications

Wenyang Zhang<sup>a,b,c</sup>, Ji Ma<sup>a,b,c,d</sup>, and Da-Wen Sun<sup>a,b,c,e</sup>

<sup>a</sup>School of Food Science and Engineering, South China University of Technology, Guangzhou, China; <sup>b</sup>Academy of Contemporary Food Engineering, South China University of Technology, Guangzhou Higher Education Mega Centre, Guangzhou, China; <sup>c</sup>Engineering and Technological Research Centre of Guangdong Province on Intelligent Sensing and Process Control of Cold Chain Foods, & Guangdong Province Engineering Laboratory for Intelligent Cold Chain Logistics Equipment for Agricultural Products, Guangzhou Higher Education Mega Centre, Guangzhou, China; <sup>d</sup>State Key Laboratory of Luminescent Materials and Devices, Center for Aggregation-Induced Emission, South China University of Technology, Guangzhou, China; <sup>e</sup>Food Refrigeration and Computerized Food Technology (FRCFT), Agriculture and Food Science Centre, University College Dublin, National University of Ireland, Dublin 4, Ireland

## ABSTRACT

Frozen foods are among the most popular food products and the development of techniques for the rapid detection of their structures and quality is important for the frozen food industry. In the current review, the principles and applications of Raman spectroscopic techniques in detecting and evaluating the structure changes and quality of frozen foods are discussed and merits and drawbacks of each Raman type are presented. These techniques include dispersive, Fourier transform, spatially offset, micro Raman spectroscopies. Raman spectroscopy can assess the compositional, physicochemical, and sensory characteristics of the frozen foods without any pretreatment. It can also be applied to investigate the structural alterations of protein, lipid, water and other components. Further trends of developing the Raman spectroscopy in monitoring the frozen foods should focus on reducing overlapping signals, achieving real noninvasive detection, eliminating misclassification and quantification errors, establishing standardized Raman database, and controlling cost.

## KEYWORDS

Food quality; authenticity; protein structure; lipid structure; water structure

## Introduction

High moisture and rich nutrition make foods highly perishable, mainly inducing microbial growth and biochemical reactions during food processing and storage. It is roughly estimated that about 25–30% of perishable fresh food products are wasted every year, and appropriate storage methods can avoid most of the waste (Coulomb 2008). Therefore, food preservation techniques such as cooling, drying, and freezing have been significantly developed to better maintain the quality of food, among them freezing technology endows foods with a longer shelf life.

In frozen foods, because of the solidification of free water, the growth and biochemical reaction of pathogenic microbial are inhibited, resulting in slow food deterioration (Li, Zhu, and Sun 2018a; Tian et al. 2020b; Zhan, Zhu, and Sun 2019; Zhu, Zhang, and Sun 2020a). However, frozen foods can also undergo some structural alterations during freezing, frozen storage, and subsequent thawing. Generally, slow freezing can produce large and unevenly distributed ice crystals outside of the cells, leading to severe frozen damage, while fast freezing often forms fine and homogeneously distributed ice crystals in the intra- and extracellular space, leading to effective alleviation of frozen damage (Ma et al.

2015; Tian et al. 2020a; Xie et al. 2015; Zhu, Zhou, and Sun 2019b). Repeated freezing-thawing cycles can also greatly affect the quality of food products due to ice crystallization and recrystallization, causing unexpected mechanical injury to tissues and cell structure (Chen et al. 2020; Qu et al. 2015a).

In general, the formation of ice crystal during freezing can cause membrane disintegration (Chen et al. 2018), leading to the changes of protein structure and the release of the main catalysts of lipid oxidation, in particular, the formation of large ice crystals can induce frozen damage, causing severe quality losses such as lipid oxidation, protein denaturation, pigment degradation, color change and flavor loss (Kang, You, and Jun 2020; Zhang and Erbjerg 2019). Therefore, it is necessary to develop rapid and efficient methods for assessing the structural changes and quality of frozen foods.

A wide range of traditional indirect and invasive methods to assess frozen foods are available, which include microbial analysis, sensory analysis methods and physico-chemical methods (Tian et al. 2020c; Xie et al. 2015), however, these methods require tedious sample treatment and long analysis time (Cheng, Nicolai, and Sun 2017; Zhou et al. 2020). On the other hand, spectroscopic analytical techniques have

been proven as valuable alternatives to rapid detection of food structure and quality. Impedance spectroscopy is an effective tool that can be used to determine meat freshness, especially to estimate the structural damage in biological tissues (Egelandsdal et al. 2019; Fuentes et al. 2013), however, the method is unable to determine the structure of frozen food components including protein, lipid, and water. Fluorescence spectroscopy mainly provides detailed information about the tertiary structures of protein, but it is unsuitable for the detection of protein secondary structures (Wang et al. 2017). Near-infrared spectroscopy is a powerful spectroscopic analytical technique for studying the secondary structure of the protein, nevertheless, the interference resulting from water is substantial (Qu et al. 2015b). Nuclear magnetic resonance (NMR) is a fundamental analytical technique that can obtain specific information about the proteins, lipids, and water, however, this technique is not suitable for detecting minor components such as low molecular weight proteins (Herrero 2008b). By contrast, Raman spectroscopy can be used for both liquid and solid samples, which can provide detailed information about molecular vibration related to secondary and tertiary structures of protein, lipid structures, and water structures (Velioglu, Temiz, and Boyaci 2015), therefore in recent years, more and more attention has been paid to the applications of Raman spectroscopic techniques for detecting the structures and quality of a wide range of food products including frozen foods.

A number of reviews on the applications of Raman spectroscopy for the food industry have been published. Herrero (2008a) summarized the applications of Raman spectroscopy for quality assessment of muscle foods based on the structural information about the alterations of protein, lipid, and water. In his other review, Herrero (2008b) only focused on the applications of Raman spectroscopy for monitoring protein structure in muscle food systems. Besides, Rygula et al. (2013) reviewed the analytical methods based on Raman spectroscopy for investigating 26 proteins with different structures, functions, and properties. However, no review is available focusing on the applications Raman spectroscopic techniques for detecting and evaluating the structure changes and quality of frozen foods. Therefore, the current review aims to collate and compare currently available publications on the topic. The techniques covered include dispersive, Fourier transform, spatially offset, micro and confocal Raman spectroscopies. In the review, the principles of these techniques are introduced, their merits and drawbacks are compared, and future trends of developing the Raman spectroscopy in monitoring frozen foods are also proposed. It is hoped that this review should attract more research interests and applications in Raman spectroscopic techniques for the frozen food industry.

## Principles of Raman spectroscopic techniques

### Raman scattering and spectroscopy

The illumination of a sample by monochromatic ultraviolet (UV), visible or near-infrared (NIR) light from a laser can cause the vibrational energy levels in the molecules from

ground electronic state to a transitory and high energy collision state, which return to a lower energy state through photon emission (Ewen and Geoffrey 2019). The majority of scattered photons have no energy interchange with the measured sample molecules and just undergo the alteration of propagation direction, demonstrating that the frequency of the scattered photon is identical with that of the incoming photon, and this phenomenon is called Rayleigh scattering or elastic scattering (Butler et al. 2016). However, a fraction of scattered photons can exchange energy with the target molecules and undergo the alteration of propagation direction and frequency. This process is known as Raman scattering or inelastic scattering (Ewen and Geoffrey 2019).

There are two types of Raman scattering, namely, Stokes scattering and anti-Stokes scattering (Figure 1A). Regarding the Stokes scattering, the energy of incoming light can be transferred to sample molecules by nuclear motion within a molecule, which causes energy loss of scattered photons and hence reduces the frequency. For the anti-Stokes scattering, the energy of a few molecules is transferred to the photon because these molecules are initially in a relatively high energy state (Ember et al. 2017). The frequency difference between the incoming light and the Raman scattered photon is referred to as Raman shift ( $\Delta\nu$  in  $\text{cm}^{-1}$ ). Furthermore, Raman scattering is a rare phenomenon with only one Raman scattered photon in every  $\sim 10^8$  of the total scattered photons (Butler et al. 2016). Thus, it is considered as an insensitive tool in comparison with inelastic scattering. Between the two aforementioned scattering types, the Stokes scattering is stronger than the anti-Stokes scattering due to the increased probability of molecule in the ground state (Butler et al. 2016). Therefore, the peak of Stokes scattering is taken as a detection peak, whereas the peak of anti-Stokes scattering is commonly neglected.

Based on Stokes scattering phenomena, Raman spectroscopic techniques are developed for detection purpose. Figure 1B shows the components of a typical Raman spectrometer, which mainly comprises laser light sources, a sample cell, a rejection filter for elastic scattering, a monochromator, and a detector. For food detection, the most frequently used laser sources are Ar laser (488.8 nm), Kr laser (568 nm), He/Ne laser (632.8 nm), and Nd:YAG (532 nm) for visible light and diode laser (785 nm) and Nd:YAG (1064 nm) for NIR light (Wang et al. 2018). As the scattering intensity is dependent on the fourth power of the frequency, the higher the frequency of the incoming light, the stronger the sensitivity of Raman spectroscopy detection, which means that the Raman signal intensity is the highest in the UV or short-wavelength visible region (Ewen and Geoffrey 2019; Jermyn et al. 2016). An advantage of UV excitation is that it has less fluorescence interference as compared with visible excitation. However, most of the food compounds can absorb UV radiation, and the high energy of a photon can usually cause the degradation of the tested sample. Therefore, NIR wavelengths, especially 785 nm, are always used to minimize the fluorescence interference issues of the sample. Additionally, the most commonly used detectors are charge-coupled devices (CCD) detector, photomultiplier tubes detector, as well as indium-gallium-arsenic compounds (InGaAs)

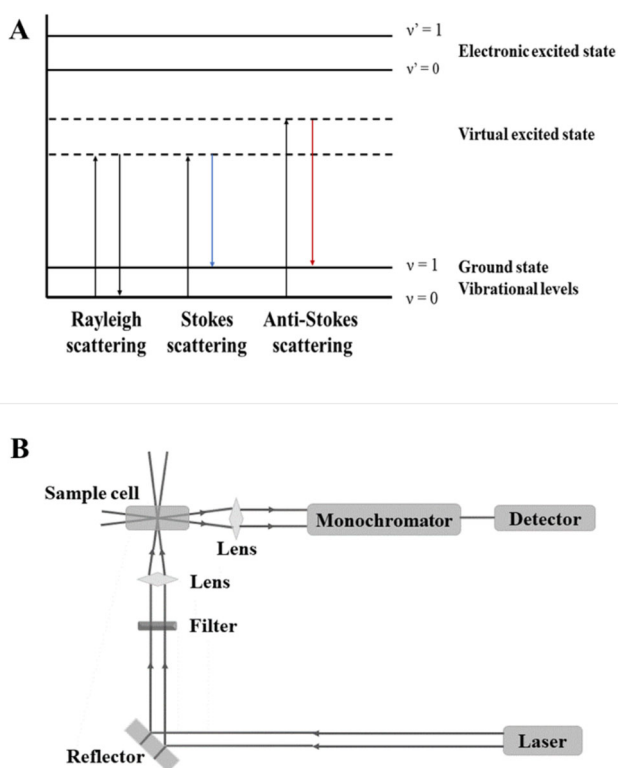


**Figure 1.** (A) Energy level transition diagram. Rayleigh scattering is also called elastic scattering, the photon energy of incoming light is the same as the scattering photon. Raman scattering is known as inelastic scattering, the photon energy of incoming light is higher than the scattering photon, called Stokes scattering; the photon energy of incoming light is lower than the scattering photon, called anti-Stokes scattering. (B) A schematic diagram of modern Raman spectrometer, which mainly comprises laser light sources, sample cell, filter, monochromator, and detector. Adapted from Wang et al. (2018).

detector (Hussain et al. 2020; He et al. 2020; Wang et al. 2018; Wu et al. 2020).

Raman and infrared spectroscopy are complementary analytical techniques as both are based on the discrete vibration transitions taking place in the ground electronic state of molecules (Thygesen et al. 2003). The requirement for vibration activity in infrared spectroscopy is a change in electrical dipole moment. In contrast, the requirement of Raman for vibration activity is a change in the electrical polarizability of the molecule (Hu et al., 2020a, 2020b; Jayan et al. 2020; Tao and Ngadi 2018; Wang et al. 2020a, 2020b). Thus, polar groups (e.g., C=O, N-H, C-H) have intense infrared bands, while nonpolar groups (e.g., C=C, C-C, S-S) have strong Raman stretching vibrations (He et al. 2019). It is worth noting that O-H stretching vibration is very strong in infrared but comparatively weak in Raman due to the weakly polarizable OH band. For this reason, compared with infrared spectroscopy, Raman spectroscopy has great advantages for detecting water-rich food as the influence of water on Raman spectra is always negligible.

Different types of Raman spectroscopy are available, and dispersive Raman spectroscopy, Fourier transform Raman spectroscopy (FT-Raman spectroscopy), spatially offset Raman spectroscopy (SORS), and micro-Raman spectroscopy are predominately used for detecting frozen foods. Table 1 summarizes these Raman spectroscopic techniques.

### Dispersive Raman spectroscopy

As the most common Raman spectroscopic technique, the intense monochromatic radiation of dispersive Raman spectroscopy is often provided by continuous-wave gas lasers, such as Ar laser (488.0, 514.5 nm), Kr (568 nm) or diodes laser (780 or 830 nm) combined with a CCD detector with a single-grating spectrograph (Yang and Ying 2011). Although strong Raman scattering can be obtained by using the laser in the visible region as the excitation light source, the intense fluorescence interference can be produced at the same time. Thus, 780 or 830 nm diodes lasers are always used to suppress the fluorescence interference from the sample.

An advantage of dispersive Raman spectroscopy is that it can be used for the detection of aqueous-phase samples (Yang and Ying 2011). Furthermore, dispersive Raman spectrometers can be miniaturized, such as hand-held Raman spectrometers. There are some issues related to dispersive Raman spectroscopy, such as thermal effect caused by laser irradiation, fluorescence interference, lack of precise frequency base, and difficulty in acquiring high-resolution spectra (Herrero 2008b; Yang and Ying 2011).

### Fourier Transform Raman Spectroscopy

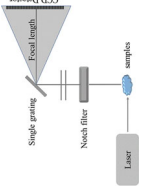
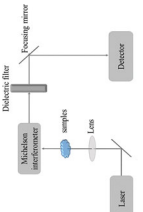
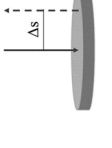
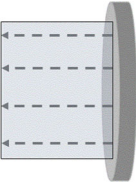
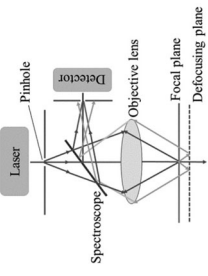
FT-Raman spectrometer, using NIR excitation sources, was first commercially employed in 1987 (Li and Church 2014). Fourier transform apparatuses operate a Michelson interferometer instead of the conventional grating monochromator, and FT-Raman spectroscopy thus has a faster collection rate and higher signal-to-noise compared with conventional spectroscopy instruments (Ma and Phillips 2002). Due to the employment of 1064 nm excitation from Nd: YAG lasers, the fluorescence interference on FT-Raman spectroscopy can be reduced to a great extent, therefore, satisfactory Raman spectra can be obtained for most organic compounds and biological samples. In addition, thermal decomposition of the tested sample caused by the laser irradiation can be avoided because the NIR wavelength is far away from the absorption band of the sample.

Compared with dispersive Raman spectroscopy, FT-Raman spectroscopy can be applied to decrease the laser-induced fluorescence interference, reduce analysis time and obtain high-resolution spectra (Wang et al. 2018; Yang and Ying 2011). For frozen foods, FT-Raman spectroscopy is mainly used to assess structural alterations of protein, because the fluorescence interference from sample surface can be minimized (Badii and Howell 2003; Schulz, Baranska, and Baranski 2005). However, the disadvantage of FT-Raman spectroscopy is the poor reproducibility caused by baseline drift (Wang et al. 2018).

### Spatially offset Raman spectroscopy

Spatially offset Raman spectroscopy (SORS) is a type of advanced Raman spectroscopic technique that collects Raman signals from subsurface layers in the tested sample

Table 1. Brief introduction of several types of Raman spectroscopies.

Techniques	Advantages	Disadvantages	Acquisition time	Spectral resolution	Depth	Schematic diagram	References
Dispersive Raman spectroscopy	Suitable for aqueous sample Inhibition of fluorescence interference at 780 or 830 nm	Thermal effect caused by laser irradiation Intense fluorescence interference Lack of precise frequency base Difficulty in acquiring high-resolution spectra Poor reproducibility caused by baseline drift	>15 s Point-based full spectrum	>12 cm <sup>-1</sup>	/		Chao et al. (2018); Herrero (2008b); Yang and Ying (2011)
Fourier transform Raman spectroscopy	Inhibition of fluorescence interference High spectra resolution Short analysis time		>2 s Point-based full spectrum	>4 cm <sup>-1</sup>	/		Careche, Herrero, and Carmona (2002); Wang et al. (2018); Yang and Ying (2011)
Spatially offset Raman spectroscopy	Suppression of fluorescence interference More depth information within the tissue	Strong absorption caused by strong absorption materials	>5 s Point-based full spectrum	>5 mm <sup>2</sup>	< 5 mm		Ember et al. (2017); Esmonde-White et al. (2017); Matousek and Stone (2016)
Micro-Raman spectroscopy	High spectral resolution Short analysis time	Slight fluorescence interference	>10 s Point-based full spectrum	>2 cm <sup>-1</sup>	/		Esmonde-White et al. (2017); Veloglu, Temiz, and Boyaci (2015); Wang et al. (2018)
Confocal Raman microscopy	High spectral resolution 2D and 3D Raman images	Baseline drift caused by long-time analysis	>1 s Point-based full spectrum	≤0.15 cm <sup>-1</sup>	≤50 μm		Camorani et al. (2015); Jermyn et al. (2016); Yang and Ying (2011)

Note: solid line represents excitation light, the dashed line represents the signal collection. The parameters thresholds (acquisition time, spectral resolution, and depth) for each Raman technique represent the best values in the literature for evaluating the quality of frozen foods.



based on spatially separating collection Raman signal zone from the laser illumination zone, as shown in Table 1 (Jermyn et al. 2016; Matousek 2018). The fundamental principle of SORS is based on the photon transfer theory. Compared with the conventional Raman, the benefit of the SORS is that the fluorescence interference from the sample surface can be reduced to a large extent (Matousek and Stone 2016). When a laser beam illuminates the surface of a tested sample, part of the Raman-scattered light reaches the subsurface layer of the sample, and Raman-scattered photons are easy to migrate from the subsurface layer than the surficial layer of the sample. The Raman-scattered photons then return to the surficial layer of the sample after elastically scattered multiple times, and the photons are collected by the collection system (Jermyn et al. 2016).

Generally, the larger the spatially offset ( $\Delta s$ ), the larger the penetration depths of the collected Raman-scattered photons (Matousek 2018). By optimizing system structure and data processing methods, and improving system detection efficiency and signal-to-noise ratio, effective collection and analysis of spectral information from deep layers of the sample can be realized.

SORS can be used to optimize the recovery of Raman signals of subsurface layers and weaken the fluorescence interferences from the sample surface. It is suitable for detecting samples with opaque/translucent surfaces or high fluorescence backgrounds, such as frozen fish (Esmonde-White et al. 2017). Additionally, the general limitation of SORS is

that samples with strong surface absorption can restrict photon diffusion, thus limiting the penetration depth (Afseth et al. 2014; Matousek 2018).

### Micro-Raman spectroscopy

This analytical technique combines the analytical characteristics of Raman spectroscopy with the visualization capability of optical microscopy, allowing for the analysis of a sample at the micron-scale (Herrero 2008b; Hubbard, Shore, and Stone 2019). Micro-Raman spectroscopy employs an epi-illumination configuration, whose microscope objective delivers not only focused laser light to the microscope but also collects Raman-scattered photons (Esmonde-White et al. 2017). It has been used for detecting the alterations of protein secondary and tertiary structures, and changes of lipid structure during freezing and thawing of foods (Gao et al. 2019; Velioglu, Temiz, and Boyaci 2015).

Confocal Raman microscopy is micro-Raman spectroscopy that combines Raman spectrometer with a confocal technique, thus Raman images with high resolutions can be obtained (Hussain et al. 2020a, 2020b, 2020c; Wang et al. 2019a, 2019b, 2019c). In confocal Raman microscopy, detailed information of a complete Raman spectrum at every image pixel can be acquired, and a lateral resolution at the diffraction limit can be achieved (Gomes da Costa et al. 2019; Hussain et al. 2019). Compared with general micro-Raman spectroscopy, confocal Raman probes can achieve

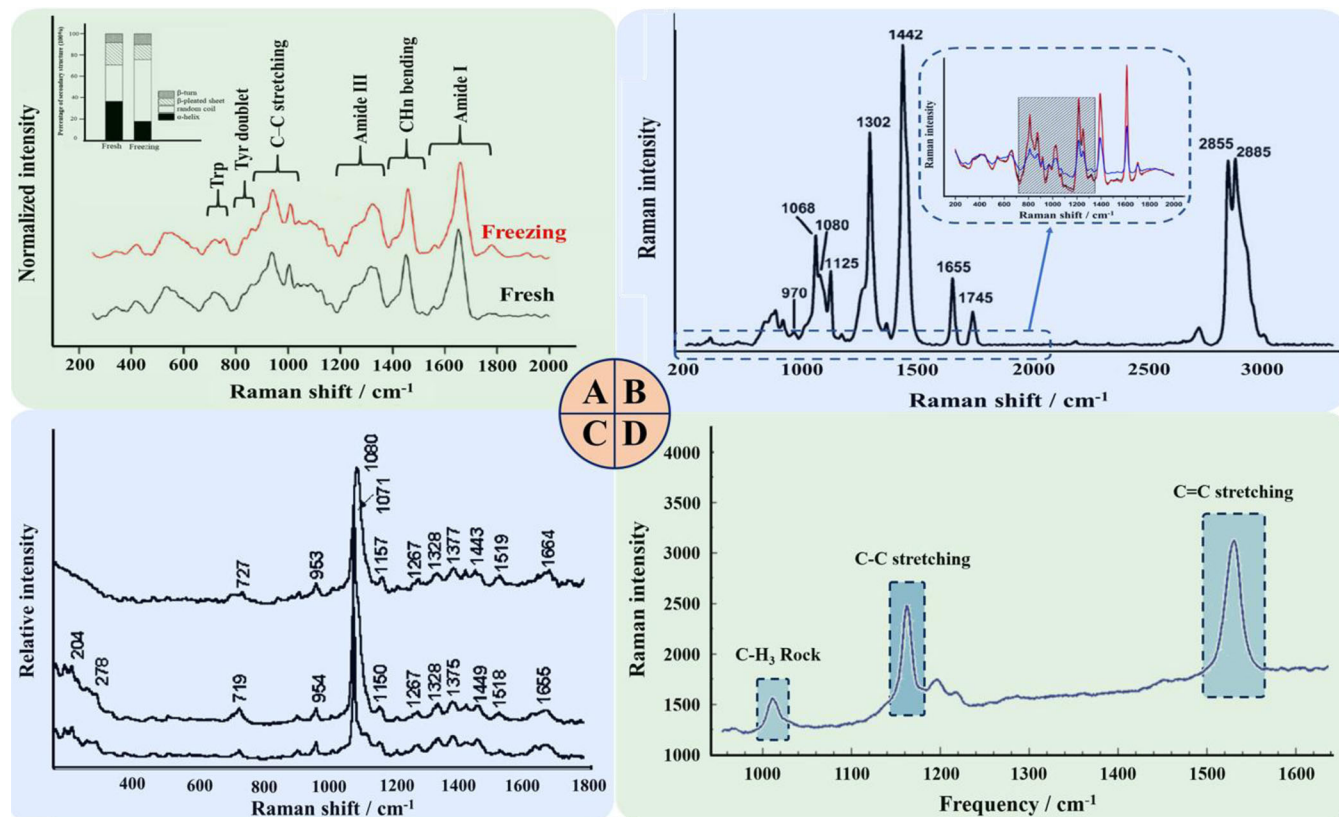


**Figure 2.** Typical Raman spectra of (A) surimi protein after frozen storage for 12 weeks in the 400–1800 cm<sup>-1</sup> region, inset: secondary structure percentage of surimi (B) frozen fish lipids in the 500–3100 cm<sup>-1</sup> region, inset: Raman spectra of fat samples extracted from horse mackerel samples (black line: fresh sample, red line: frozen-thawed sample (1 cycle), blue line: frozen-thawed sample (2 cycles), (C) Argentine red shrimp shell in the 150–1800 cm<sup>-1</sup> region, top to bottom: a control, the outer and inner side of white-spot, and (D) frozen raw and cooked carrot slices in the 1000–1600 cm<sup>-1</sup> region. Adapted from Careche, Herrero, and Carmona (2002); Chen et al. (2018); Gao et al. (2019) and Camorani et al. (2015).

**Table 2.** Useful Raman modes in the interpretation of the structure of proteins, lipids and water.

Types	Origins	Raman shift (cm <sup>-1</sup> )	Assignment	Relevant information	References
Proteins	Cysteine	510	S-S stretching	Gauche-gauche-gauche conformation	Gao et al. (2019); Krimm and Bandekar (1986)
		525	S-S stretching	Gauche-gauche-trans conformation	
		545	S-S stretching	Trans-gauche-trans conformation	
	Cysteine, methionine	655, 724	C-S stretching	Trans conformation	Schmidt, Scheier, and Hopkins (2013)
		700	C-S stretching	Gauche conformation	
	Tyrosine	2550-258	S-H stretching	Cysteinyl residues	Yu, Jo, and O'Shea (1973); Kang et al. (2014); Zhou et al. (2019)
		850/830	Fermi resonance between ring fundamental and overtone	State of the phenolic hydroxyl group (exposed or buried, hydrogen-bond donor or acceptor, hydrophobic or hydrophilic environment)	
				Sensitive to environment polarity	
				Conformation insensitive, used for normalizing the spectra	
	Tryptophan	760, 880, 1340, 1360	Indole-ring	Environment insensitive	Chen et al. (2020); Li-Chan (1996)
Phenylalanine	1002-1006	Ring breathing	Monitor the ionization state in D <sub>2</sub> O solutions	Herrero (2008b); Schmidt, Scheier, and Hopkins (2013)	
			Ionized COO <sup>-</sup> groups	Li-Chan (1996); Zhao, Downey, and O'Donnell (2015)	
			Undissociated COOH	Sánchez-González et al. (2008)	
			C-C stretching		
			C-C stretching		
			C-H bending		
			C-H stretching		
			C=O stretching, N-H bending		
			C=O stretching, N-H bending		
			C=O stretching, N-H bending		
			N-H in-plane bending, C-N stretching		
			N-H in-plane bending, C-N stretching		
			N-H in-plane bending, C-N stretching		
			N-H in-plane bending, C-N stretching		
			N-H in-plane bending, C-N stretching		
			N-H in-plane bending, C-N stretching		
			N-H in-plane bending, C-N stretching		
			N-H in-plane bending, C-N stretching		
			N-H in-plane bending, C-N stretching		
			N-H in-plane bending, C-N stretching		
			N-H in-plane bending, C-N stretching		
			N-H in-plane bending, C-N stretching		
			N-H in-plane bending, C-N stretching		
			N-H in-plane bending, C-N stretching		
			N-H in-plane bending, C-N stretching		
			N-H in-plane bending, C-N stretching		
			N-H in-plane bending, C-N stretching		
			N-H in-plane bending, C-N stretching		
			N-H in-plane bending, C-N stretching		
			N-H in-plane bending, C-N stretching		
			N-H in-plane bending, C-N stretching		
			N-H in-plane bending, C-N stretching		
			N-H in-plane bending, C-N stretching		
			N-H in-plane bending, C-N stretching		
			N-H in-plane bending, C-N stretching		
			N-H in-plane bending, C-N stretching		
			N-H in-plane bending, C-N stretching		
			N-H in-plane bending, C-N stretching		
			N-H in-plane bending, C-N stretching		
			N-H in-plane bending, C-N stretching		
			N-H in-plane bending, C-N stretching		
			N-H in-plane bending, C-N stretching		
			N-H in-plane bending, C-N stretching		
			N-H in-plane bending, C-N stretching		
			N-H in-plane bending, C-N stretching		
			N-H in-plane bending, C-N stretching		
			N-H in-plane bending, C-N stretching		
			N-H in-plane bending, C-N stretching		
			N-H in-plane bending, C-N stretching		
			N-H in-plane bending, C-N stretching		
			N-H in-plane bending, C-N stretching		
			N-H in-plane bending, C-N stretching		
			N-H in-plane bending, C-N stretching		
			N-H in-plane bending, C-N stretching		
			N-H in-plane bending, C-N stretching		
			N-H in-plane bending, C-N stretching		
			N-H in-plane bending, C-N stretching		
			N-H in-plane bending, C-N stretching		
			N-H in-plane bending, C-N stretching		
			N-H in-plane bending, C-N stretching		
			N-H in-plane bending, C-N stretching		
			N-H in-plane bending, C-N stretching		
			N-H in-plane bending, C-N stretching		
			N-H in-plane bending, C-N stretching		
			N-H in-plane bending, C-N stretching		
			N-H in-plane bending, C-N stretching		
			N-H in-plane bending, C-N stretching		
			N-H in-plane bending, C-N stretching		
			N-H in-plane bending, C-N stretching		
			N-H in-plane bending, C-N stretching		
			N-H in-plane bending, C-N stretching		
			N-H in-plane bending, C-N stretching		
			N-H in-plane bending, C-N stretching		
			N-H in-plane bending, C-N stretching		
			N-H in-plane bending, C-N stretching		
			N-H in-plane bending, C-N stretching		
			N-H in-plane bending, C-N stretching		
			N-H in-plane bending, C-N stretching		
			N-H in-plane bending, C-N stretching		
			N-H in-plane bending, C-N stretching		
			N-H in-plane bending, C-N stretching		
			N-H in-plane bending, C-N stretching		
			N-H in-plane bending, C-N stretching		
			N-H in-plane bending, C-N stretching		
			N-H in-plane bending, C-N stretching		
			N-H in-plane bending, C-N stretching		
			N-H in-plane bending, C-N stretching		
			N-H in-plane bending, C-N stretching		
			N-H in-plane bending, C-N stretching		
			N-H in-plane bending, C-N stretching		
			N-H in-plane bending, C-N stretching		
			N-H in-plane bending, C-N stretching		
			N-H in-plane bending, C-N stretching		
			N-H in-plane bending, C-N stretching		
			N-H in-plane bending, C-N stretching		
			N-H in-plane bending, C-N stretching		
			N-H in-plane bending, C-N stretching		
			N-H in-plane bending, C-N stretching		
			N-H in-plane bending, C-N stretching		
			N-H in-plane bending, C-N stretching		
			N-H in-plane bending, C-N stretching		
			N-H in-plane bending, C-N stretching		
			N-H in-plane bending, C-N stretching		
			N-H in-plane bending, C-N stretching		
			N-H in-plane bending, C-N stretching		
			N-H in-plane bending, C-N stretching		
			N-H in-plane bending, C-N stretching		
			N-H in-plane bending, C-N stretching		
			N-H in-plane bending, C-N stretching		
			N-H in-plane bending, C-N stretching		
			N-H in-plane bending, C-N stretching		
			N-H in-plane bending, C-N stretching		
			N-H in-plane bending, C-N stretching		
			N-H in-plane bending, C-N stretching		
			N-H in-plane bending, C-N stretching		
			N-H in-plane bending, C-N stretching		
			N-H in-plane bending, C-N stretching		
			N-H in-plane bending, C-N stretching		
			N-H in-plane bending, C-N stretching		

3	~3250 ~3470 ~3630	Hydrogen-bonded components Hydrogen-bonded components Hydrogen-bonded components	Strongly bonding Weakly bonding Slightly bonding Bound water Mobile water Most mobile water	Dong et al. (2007)
	3100–3250 3250–3420 3420–3620	O–H stretching O–H stretching O–H stretching		Boireau-Adamezyk, Baillet-Guffroy, and Stamatas (2014)
5	3070 3218 3408 3541 3630 3051, 3233, 3393 3511, 3628	DAA–OH DAA–OH DA–OH DDA–OH Free–OH Hydrogen bonding Non-hydrogen bonding		Li, Zhu, and Sun (2020b)
			water molecule water molecule	Dou et al. (2020)

acquisition time as fast as 1 s. The field-of-view of 2D images produced by raster-scanning confocal Raman microscopy is typically between 0.01 and 1 mm<sup>2</sup>. Moreover, confocal Raman microscopy with excellent depth resolution can be used to acquire 3D Raman images and depth profiles.

Confocal Raman microscopy can be employed to analyze targets through glass containers, plates, and aqueous samples with little hindrance, thus focusing directly on the content to extract chemical fingerprints (Teixeira Dos Santos et al. 2017), and has been employed for exploring the spatial distribution of food components such as starch, gluten, arabinoxylan. More importantly, confocal Raman microscopy has an ability to determine the size and distribution of ice crystals during freezing and recrystallization and assess the interaction between water and other components of frozen foods (Huen et al. 2014).

### Detection of structures of frozen food components

Previous studies have indicated that the formation of ice crystal during freezing can result in membrane disintegration (Chen et al. 2018) and causes changes in protein structures and releases the main catalysts for lipid oxidation. Raman spectroscopic techniques can acquire nondestructively specific information on the structure of molecular vibrations of food samples, and thus can be used to elucidate the structural changes of protein, determine lipid oxidations process and investigate interactions of protein-protein or protein-lipid (Sanchez-Alonso, Carmona, and Careche 2012; Sarkardei and Howell 2007).

### Protein structures

The Raman spectral assignment of vibration bands of proteins is based on model compounds such as amino acid or short peptides. Besides, Raman spectra can acquire information about protein modifications in secondary structures (amide I and amide III region, C–C stretching band) and changes in protein local environment (tyrosyl doublet, tryptophan residues, and aliphatic side chains). Figure 2A and Table 2 show some useful information for interpreting protein structures.

### Protein secondary structure

Amide conformation region including amide I (1600–1700 cm<sup>−1</sup>), amide II (1510–1560 cm<sup>−1</sup>) and amide III (1230–1350 cm<sup>−1</sup>) bands are almost used to provide useful information about the changes of the protein secondary structure (e.g.,  $\alpha$ -helix,  $\beta$ -pleated sheet,  $\beta$ -bend, random coil).

The amide I band involves mainly C=O stretching, and to a lesser extent, C–N stretching, N–H in-plane bending and C $\alpha$ –C–N bending of the peptide group (Li-Chan 1996). Some research results exhibited that amide I band was related to the amount of the types of protein backbone conformation (Herrero 2008b; Rygula et al. 2013). In general, the bands of  $\alpha$ -helix,  $\beta$ -pleated sheet,  $\beta$ -turn, and random coil or disorder structure are located at 1645–1660, 1665–1680, 1680–1690, and 1665–1670 cm<sup>−1</sup>, respectively.



The location of the amide I band depends on the hydrogen bonding (H-bonding) and conformation of protein structure, and the regions that are sensitive to change in H-bonding scheme involves peptide linkages (Herrero 2008a). Moreover, the differences in the content of the protein secondary structure can affect its spectral peak pattern in the amide I region.

The amide II mode involves N-H in-plane bending and C-N stretching of the peptide group (Ewen and Geoffrey 2019), but it always has important contributions from C-C stretching and smaller contributions from C-N stretching (Krimm and Bandekar 1986). The small variation in polarizability associated with the amide II makes it difficult to be measured on factual research, therefore, this region is generally not used in studies (Herrero 2008b).

The amide III vibration mainly involves C-N stretching and N-H in-plane bending of the peptide group. Commonly, a protein with high contents of  $\alpha$ -helical structure possesses a weak band, located between 1260 and  $\text{cm}^{-1}$ .  $\beta$ -pleated sheet structure generates a more intense band near 1230–1240  $\text{cm}^{-1}$ , while the random coil structure appears in 1240–1255  $\text{cm}^{-1}$  range. The bands of  $\beta$ -pleated sheet and random coil are overlapped to some extent in Raman spectra, which makes the amide III band challenging to be interpreted by vibrational spectroscopy of proteins (Krimm and Bandekar 1986; Herrero 2008b; Rygula et al. 2013).

C-C stretching vibrations are also employed to acquire information about the secondary structure of the protein. The location of C-C stretching bands in the 890–1060  $\text{cm}^{-1}$  range, which are characteristic of  $\alpha$ -helix at 890–945  $\text{cm}^{-1}$  and  $\beta$ -pleated sheet at 1020–1060  $\text{cm}^{-1}$  (Li-Chan 1996; Cai et al. 2019; Sun et al. 2011). The C-C stretching vibrations in the carbon chains skeleton lead to changes in the Raman peak near 940  $\text{cm}^{-1}$ , which is a crucial embodiment for  $\alpha$ -helix structure in Raman spectra (Krimm and Bandekar 1986).

### Protein local environments

Raman bands at 760, 880, 1340, and 1360  $\text{cm}^{-1}$  are assigned to the indole ring vibrations of tryptophan residues, which can offer information about the tertiary structure of protein local environment (Krimm and Bandekar 1986; Li-Chan 1996). Some studies on protein Raman bands reveal that the decrease of peak intensity at 760  $\text{cm}^{-1}$  is caused by the exposure of buried tryptophan residues in proteins (Herrero 2008b; Schmidt, Scheier, and Hopkins 2013).

The doublet bands, centered at 830 and 850  $\text{cm}^{-1}$ , are assigned to Fermi resonance between ring fundamental and overtone of tyrosine residues, which is a good indicator of H-bonding of the phenolic OH group. The tyrosyl doublet ratio ( $I_{850}/I_{830}$ ) can be used to reflect “buried” and “exposed” tyrosine groups, and thus become an effective probe for monitoring the microenvironment of tyrosine residues (Yu, Jo, and O’Shea 1973; Zhou et al. 2019; Zhu et al. 2019). If  $I_{850}/I_{830}$  falls in between 0.7–1.0, the tyrosine residues are considered as “buried”, indicating that the hydrophobic groups of tyrosine gather with each other to form hydrophobic nuclei and are buried in the peptide chain. By

contrast, if  $I_{850}$  is higher than  $I_{830}$ , tyrosine residues are exposed on the protein surface.

Raman bands at 1440–1465  $\text{cm}^{-1}$  and 2800–3000  $\text{cm}^{-1}$  are assigned to  $\text{CH}_2$  and  $\text{CH}_3$  bending and C-H stretching vibrations of aliphatic residues, respectively. Some research reported that the intensity near 2930  $\text{cm}^{-1}$  band increased with increasing polarity of the microenvironment around the hydrocarbon chain (Kang et al. 2014; Krimm and Bandekar 1986; Zhang et al. 2016).

Phenylalanine shows ring breathing modes near 1002–1006  $\text{cm}^{-1}$  and is insensitive to protein conformation or microenvironment. Therefore, it can be used as an internal standard for the normalization of the protein Raman spectra (Herrero 2008b; Zhu et al. 2019a). Disulfide bonds of cystine residues show Raman bands near 510, 525, and 545  $\text{cm}^{-1}$ , which are assigned to gauche-gauche-gauche (g-g-g), gauche-gauche-trans (g-g-t), and trans-gauche-trans (t-g-t) conformations, respectively (Krimm and Bandekar 1986; Li-Chan 1996). The exact location of Raman bands of cystine residues depends on the conversion of sulfhydryl/disulfide bonds within and between molecules. In addition, Raman bands of C-S bond of the cysteine and methionine residues, S-H group of cysteinyl residues, histidine residues, as well as aspartic and glutamic acids residues can also provide information about the tertiary structure of the protein.

### Lipid structure

The fatty acid profile is an important factor for the assessment of lipids. The intensity and location of lipids Raman bands depend on the fatty acid compositions and their degree of saturation. Some useful information about lipids Raman modes for the interpretation of lipids structure is exhibited in Table 2. A typical lipid Raman spectrum of frozen fish is depicted in Figure 2B, showing that typical lipid Raman bands are located at 800–1800 and 2800–3000  $\text{cm}^{-1}$  regions.

The range of 800–1800  $\text{cm}^{-1}$  is the fingerprint region of Raman spectra. Raman bands at 869, 925, and 970  $\text{cm}^{-1}$  are assigned to various CCC stretches (Li-Chan 1996; Sanchez-Alonso, Carmona, and Careche 2012). Raman bands near 1068, 1080, and 1125  $\text{cm}^{-1}$  are attributed to out-of-phase CCC stretch, anti-symmetric CCC stretch and in-phase CCC stretch, respectively. The 1200–1600  $\text{cm}^{-1}$  range shows some bands associated with the following groups:  $\delta(\text{C-H})$  symmetric rock (cis) at 1265  $\text{cm}^{-1}$ , C-H bending/twisting of the methylene at 1302  $\text{cm}^{-1}$ , and  $\delta(\text{C-H})$  scissoring of methylene at 1442  $\text{cm}^{-1}$ . It is worth noting that the intensity ratio of  $I_{1265}/I_{1302}$  is used for the rapid measurement of the total cis isomer in oil (Sarkardei and Howell 2007). The next region (1600–1800  $\text{cm}^{-1}$ ) shows two bands, with one nears 1655  $\text{cm}^{-1}$  corresponding to the cis C=C stretching and the other near 1745  $\text{cm}^{-1}$  relevant to the C=O stretching of ester. Numerous researches reported that the intensity ratios of  $I_{1665}/I_{1442}$  and  $I_{1665}/I_{1745}$  have remarkable correction with the iodine value, which stands for the total degree of unsaturated fatty acids (Herrero 2008b; Zhao, Downey, and O’Donnell 2015).

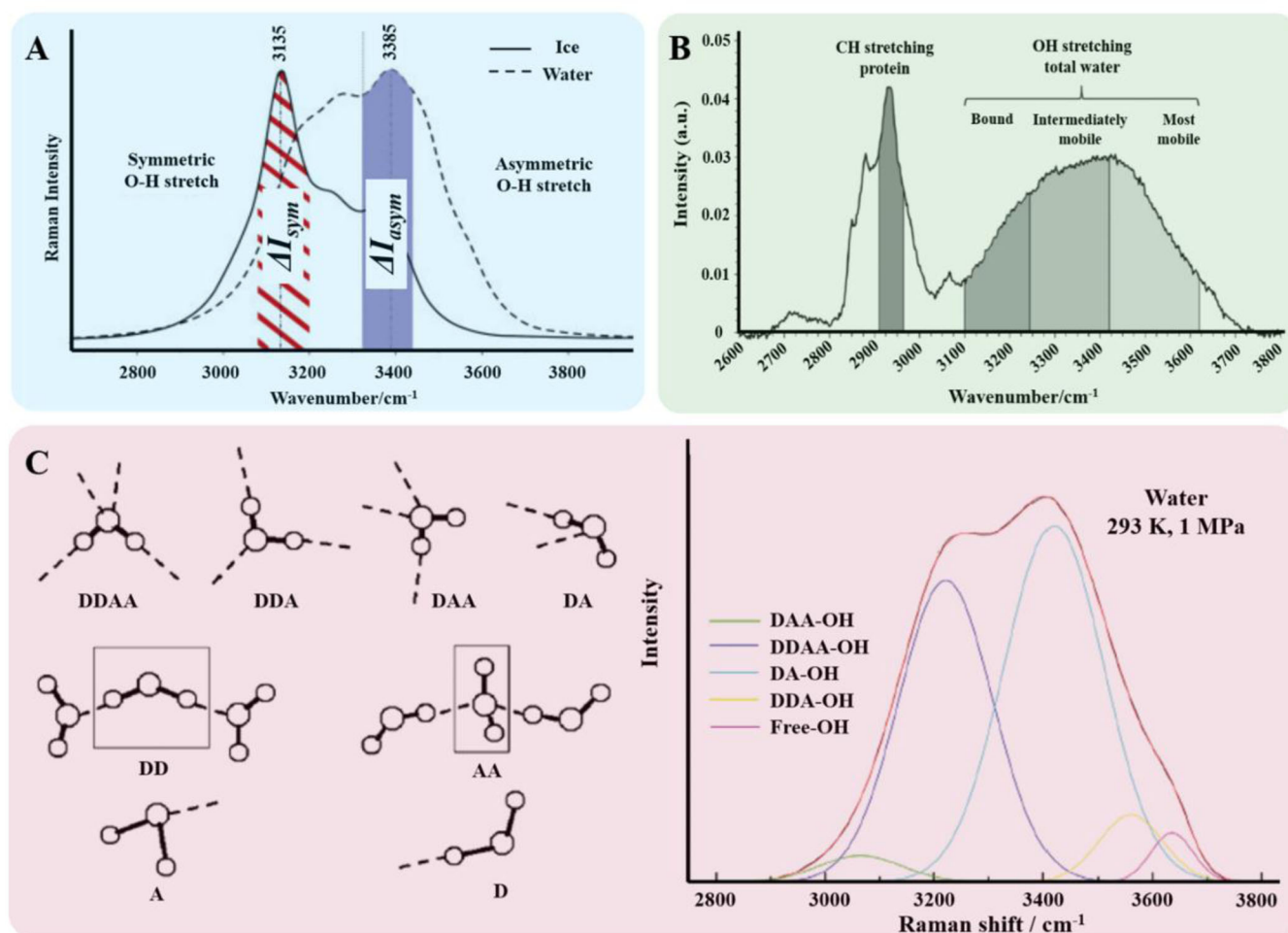


**Figure 3.** Division of Raman modes of the O–H stretching of water based on the number of sub-peaks in the range of 3000–3700  $\text{cm}^{-1}$ . (A) O–H stretching of water with 2 sub-peaks, (B) O–H stretching of water with 3 sub-peaks, (C) O–H stretching of water with 5 sub-peaks. Adapted from Boireau-Adamezyk, Baillet-Guffroy, and Stamatas (2014); Đuričković et al. (2011) and Li et al. (2020b).

The changes of Raman bands in 2800–3000  $\text{cm}^{-1}$  region are related to the modifications of C–H stretching vibrations. Therefore, Raman bands near 2855, 2931, and 2885  $\text{cm}^{-1}$  are attributed to  $\text{CH}_2$  symmetric stretching,  $\text{CH}_2$  anti-symmetric stretching, and  $\text{CH}_3$  symmetric stretching motion, respectively (Li-Chan 1996; Sanchez-Alonso, Carmona, and Careche 2012).

### Water structure

Raman spectroscopy can also be used to illuminate the structure of water in complex frozen food systems, such as frozen dough. The Raman spectra of water can be divided into three zones: the librational/translational motion bands below 600  $\text{cm}^{-1}$ , the O–H bending bands around 1580–1640  $\text{cm}^{-1}$ , as well as the O–H stretching bands fall in 3000–3700  $\text{cm}^{-1}$  regions (Carey and Korenowski 1998; Đuričković et al. 2011). Although the structure of water has been extensively studied, some results are still controversial, and Raman spectral information is useful in the interpretation of water structure. Table 2 summarizes the Raman modes relevant to water structure. Đuričković et al. (2011) assigned Raman bands around 3080–3200  $\text{cm}^{-1}$  assigned to the O–H symmetric stretching of ice and bands near

3300–3420  $\text{cm}^{-1}$  to the O–H asymmetric stretching of liquid water (Figure 3A).

As H-bonding in liquid water plays a vital role in physicochemical properties, and the changes of H-bonding directly affect the O–H stretching vibration, O–H vibrations can thus be used to study the H-bonding (Sun 2009). According to the shape of the O–H asymmetric stretching region of liquid water, Ratcliffe and Irish (1982) assigned the Raman band around 3230–3260  $\text{cm}^{-1}$  to Fermi resonance between overtone of the bending mode and O–H stretching, and the band near 3450  $\text{cm}^{-1}$  and 3630  $\text{cm}^{-1}$  to O–H symmetric stretching and O–H asymmetric stretching of water, respectively.

In order to further study the structure of water in different conditions, information about the hydrogen-bonded O–H stretching bands of water can be obtained by deconvoluting the Raman spectra of O–H stretching bands into several sub-peaks (Li, Zhu, and Sun 2020b). Sun (2009) combined Raman spectroscopy with Gaussian function to determine the local hydrogen-bonded network of water molecules. As shown in Fig 3C, the main local H-bonding for a molecule could be divided into five categories under the ambient condition, including single donor-single acceptor (DA), single donor-double acceptor (DAA), double donor-

Table 3. Applications of Raman spectroscopic techniques in frozen food systems.

Category	Samples	Analytes	Raman technique	Spectral range (cm <sup>-1</sup> )	Applications	References
Aquatic products	Red sea bream	Myofibrillar protein		400–3600	Assessment of the structural alterations of myofibrillar proteins	Nian et al. (2019)
	Red sea bream	Myofibrillar protein		400–3600	Measurement of the protein secondary and tertiary structures	Cai et al. (2019)
	Red sea bream	Myofibrillar protein			Evaluation of the protein conformational changes	Cao et al. (2018)
	Atlantic salmon	Lipid	Micro-Raman spectroscopy	200–2000	Analysis of fish freshness	Velioglu, Temiz, and Boyaci (2015)
	Salmon	Lipid, carotenoid	Spatially Offset Raman Spectroscopy	500–1800	Characterization of quality traits of fish through the skin	Afseth et al. (2014)
	Hake	Lipid	FT-Raman spectroscopy	90–4000	Analysis and characterization of hake lipids and investigation lipid alterations	Sanchez-Alonso, Carmona, and Careche (2012)
	Lizardfish	Actomyosin	FT-Raman spectroscopy		Evaluation of the protein conformational changes	Leelapongwattana et al. (2008)
	Hake	Protein	FT-Raman spectroscopy		Study of the structural alterations of muscle protein during frozen storage	Herrero, Carmona, and Careche (2004)
	Cod	Collagen	FT-Raman spectroscopy	400–3600	Elucidation of the effect of lipids on frozen stored Cod collagen	Badii and Howell (2003)
	Cod	protein	FT-Raman spectroscopy	400–3600	Investigation of the role of antioxidants and cryoprotectants in minimizing protein denaturation	Badii and Howell (2002)
Meats	Argentine red shrimp	Calcium carbonate	FT-Raman spectroscopy	650–3100	Identification of the chemical changes of shell components during frozen storage	Careche, Herrero, and Carmona (2002)
	Surimi	Protein, water	FT-Raman spectroscopy		Study of the structural alterations of water and protein	Sánchez-González et al. (2008)
	Surimi	Myofibrillar protein	Micro-Raman spectroscopy	250–2000	Assessment of the structural alterations of surimi	Gao et al. (2019)
	Surimi	Protein		500–1800	Evaluation of the protein structural alterations of surimi	Zhou et al. (2017)
	Chinese Yellow bulls	Protein, lipid	Portable Raman spectroscopy	100–3300	Prediction of the texture of different frozen/thawed raw beef	Chen et al. (2020)
	Beef	Lipid	Portable Raman spectroscopy	100–3300	Characterization of the lipid oxidation process	Chen et al. (2018)
	Young dairy bull beef	Protein, lipid		250–3380	Assessment of physic-chemical properties related to eating quality	Nian et al. (2017)
	Beefburgers	Protein, lipid	Dispersive Raman Spectroscopy	900–1800	Detection of offal adulteration	Zhao, Downey, and O'Donnell (2015)
	ovine <i>m. semimembranosus</i>	Protein, lipid	Hand-held Raman spectroscopy		Prediction of the quality traits of sheep meat	Fowler et al. (2015)
	Pork	Lipid		200–1800	Prediction of total fatty acid parameters and individual fatty acids	Berhe et al. (2016)
Others	Bread dough	Liquid water, ice, gluten	Confocal Raman microscopy		Investigation of the microstructure of bread dough and assessment of the interaction between water and other components of frozen bread dough	Huen et al. (2014)
	Carrot	carotenoid	Confocal Raman microscopy		Evaluation of carotenoid alterations after thermal treatment of carrots	Camorani et al. (2015)

single acceptor (DDA), double donor-double acceptor (DDAA), and free OH vibrations. The results indicated that O–H stretching region of water at 293 K and 0.01 MPa could be deconvoluted into five sub-peaks, which centered at 3014, 3226, 3432, 3572 and 3636  $\text{cm}^{-1}$ , corresponding to  $\nu_{\text{DAA-OH}}$ ,  $\nu_{\text{DDAA-OH}}$ ,  $\nu_{\text{DA-OH}}$ ,  $\nu_{\text{DDA-OH}}$ , and free  $\text{OH}_2$  symmetric stretching vibrations, respectively. Other studies (Boireau-Adamezyk, Baillet-Guffroy, and Stamatias 2014; Dou et al. 2020; Dong et al. 2007; Huen et al. 2014) on the structures of water indicated that the O–H symmetric stretching could be deconvoluted into two, three, and five sub-peaks, as illustrated in Figure 3 and Table 3.

### Other structures

In addition to proteins, lipids, and water, carbonate crystals in the exoskeleton of crustacean species are also key factors affecting the quality of frozen foods. Because of the high polarizability of the polyatomic inorganic anions, Raman spectroscopy is a very useful tool for studying inorganic compounds. Besides, due to the difference of crystal fields, the vibrational modes of the same character produced by two polyatomic inorganic anions with different crystal forms may appear at different frequencies (Careche, Herrero, and Carmona 2002). On this basis, Raman spectroscopy can be used to distinguish different crystal forms of carbonate.

Carbonate ions ( $\text{CO}_3^{2-}$ ) are considered to be a planar  $\text{XY}_3$  symmetric molecule, which exhibits three Raman-active vibration modes (Figure 2C). The Raman-active band with strong intensity is produced by symmetric stretching mode, falling in the 1100–1050  $\text{cm}^{-1}$  range. The asymmetric stretching mode generates a feeble Raman band, appearing in the 1500–1400  $\text{cm}^{-1}$  region. Moreover, the in-plane bending mode is weak-to-medium and appears at the 650–750  $\text{cm}^{-1}$  region. The out-of-plane bending mode appears when the  $\text{XY}_3$  planar symmetry of  $\text{CO}_3^{2-}$  is broken by the crystal field, and this band is very weak and seems in the 850–900  $\text{cm}^{-1}$  range (Careche, Herrero, and Carmona 2002). In addition to stretching and bending vibrations, the lattice vibrations band of  $\text{CO}_3^{2-}$  ion appears below the 300  $\text{cm}^{-1}$  range. Based on studying  $\text{CO}_3^{2-}$  ion, the Raman spectrum of calcium carbonates in different crystal forms can be analyzed.

On the other hand, carotenoids, as a type of essential pigment, are widely found in various food matrices, including meat, vegetables, and fruits. As shown in Figure 2D, carotenoids show Raman bands at 1008, 1155, and 1525  $\text{cm}^{-1}$  that are attributed to the rocking motion of molecule methyl (in-plane C–H<sub>3</sub> rock), the polyene chain C–C stretching vibrations, and the C=C stretching of polyene backbone, respectively (Camorani et al. 2015). Carotenoids can be identified by comparing Raman shifts in the main spectral bands, which are related to the presence of specific end-groups and/or molecular conjugation length (Camorani et al. 2015; Schulz, Baranska, and Baranski 2005)

## Detection of quality of frozen foods

With Raman band assignments for proteins, lipids, water and other compounds, Raman spectroscopy has been extensively used for analyzing the quality of frozen foods. Table 3 presents these applications.

### Frozen aquatic products

Despite the wide use of freezing and frozen storage for inhibiting microbial activity, prolonging shelf life and reducing deterioration rate for aquatic products, freezing can induce protein denaturation, loss of protein functionality as well as lipid oxidation due to possible mechanical damages caused by ice crystal formation in frozen aquatic products. For protein, changes in Raman shift and Raman band intensity are commonly used as indicators for alterations in protein secondary structure and microenvironment, and amide I and amide III bands can provide information regarding protein secondary structures.

In general,  $\alpha$ -helix and  $\beta$ -pleated sheet stand for the conformation regularity of protein, while  $\beta$ -turn and random coil indicate the conformation looseness of protein (Cai et al. 2019). A decrease in the percentages of the  $\alpha$ -helical structure normally indicates the generation of a partial denaturation of the proteins. Cao et al. (2018) reported that the percentage of random coil tended to increase while the percentages of  $\alpha$ -helix and  $\beta$ -pleated sheet tended to decrease with increasing freezing-thawing cycles, manifesting that the original structures of the protein were gradually lost. The same result was obtained by Gao et al. (2019) as shown in Figure 2A, indicating increases in the percentages of random coil and  $\beta$ -turn increased while decreases in the percentages of  $\alpha$ -helix and  $\beta$ -pleated sheet after frozen storage of the surimi for 12 weeks. In addition, the intensity of 760  $\text{cm}^{-1}$  and the intensity ratio of tyrosine doublet ( $I_{850}/I_{760}$ ) can be used to monitor the alterations of microenvironments. Zhou et al. (2017) studied the effect of camellia tea oil on the surimi gel protein secondary structure and showed that with an increase in the oil concentration, the relative intensity of 760  $\text{cm}^{-1}$  increased while the relative intensity of  $I_{850}/I_{760}$  decreased, indicating that the presence of oil could give rise to the exposure of hydrophobic groups and modify the local environment of proteins.

For lipid, the intensity of 1655  $\text{cm}^{-1}$  and the intensity ratios of  $I_{1655}/I_{1442}$  and  $I_{1655}/I_{1745}$  are regarded as the main indicator of the degree of unsaturation of lipids (Sarkardei and Howell 2007). Moreover, bands at 970 and 1080  $\text{cm}^{-1}$  have a negative correlation with the degree of saturation of lipids, and 1068 and 1125  $\text{cm}^{-1}$  have a positive relationship (Berhe et al. 2016). Sanchez-Alonso, Carmona, and Careche (2012) reported that the alteration in the 1655  $\text{cm}^{-1}$  band corresponding to conjugated dienes development was the only spectroscopic change related to hake lipid oxidation during frozen storage. The same conclusion was obtained by Velioglu, Temiz, and Boyaci (2015), showing that in the range of 1600–1660  $\text{cm}^{-1}$  band the Raman intensity changed significantly with increasing the freezing time, as seen in the inset of Figure 2B. In general, the specific changes of the



Raman intensity in the range of 1600–1660  $\text{cm}^{-1}$  depend on the types of oils. According to previous reports, this intensity increases with oxidation for sunflower, safflower or corn oils, whereas decreases for olive oil under the same conditions (Muik et al. 2005; Sanchez-Alonso, Carmona, and Careche 2012).

Afseth et al. (2014) investigated the potential of using SORS to qualify and quantify the quality parameters of intact salmon. By employing spatial offset in the range of 5–6 mm, they obtained detailed information about carotenoid content and fatty acid profile from both dark and light parts of salmon skin. More importantly, the main prerequisite of their experiment was to choose a laser resource in the NIR region.

For crustacean, a severe quality issue during frozen storage is the formation of white spots on the shell, which affects not only their appearance but also market prices. Careche, Herrero, and Carmona (2002) used Raman spectroscopy to identify the chemical components of white spots on red shrimp shell and indicated that the main calcium carbonate crystals formed on the outer shell side were ikaite and calcite, while ikaite was formed on the inner side. Also, there were no significant chitin and/or proteins conformation alterations accompanying the ikaite precipitate.

### Frozen raw meat and meat products

In order to predict texture attributes related to eating quality of beef, Nian et al. (2017) employed Raman spectroscopy and chemometrics to evaluate effects of different freezing/thawing cycles for raw beef and showed that Raman spectroscopy had good potential for prediction chewiness, tenderness, firmness, and hardness, while poor prediction ability for springiness. Moreover, principal component analysis (PCA) loading plots for the first principal component (PC1) and the second principal component (PC2) indicated that the prediction of the texture of frozen/thawed beef was primarily influenced by the modifications in secondary structure composition and hydrophobic characteristics of the protein.

In addition, many studies have confirmed that Raman spectroscopy had a potential to determine lipid oxidations process (Chen et al. 2018), assess protein structural alterations (Sun et al. 2011), and predict different quality traits including Warner-Bratzler shear force (WBSF) (Schmidt, Scheier, and Hopkins 2013), moisture content, cook loss (Nian et al. 2017), and pH (Fowler et al. 2015). For the prediction of WBSF values, Nian et al. (2017) and Schmidt, Scheier, and Hopkins (2013) reported that Raman spectroscopy had the ability to predict WBSF values, while inconsistent results were obtained by Fowler et al. (2015). The reason for the different results might be due to the differences in experimental design and parameters.

As Raman spectral data in the fingerprint region contain numerous information regarding the structures of protein, lipid, and water, Raman spectroscopy has the potential for addressing meat authenticity issues. Zhao, Downey, and O'Donnell (2015) reported that dispersive Raman

spectroscopy and multivariate data analysis were used to determine offal adulteration in thawed beef burgers. Partial least-squares-discriminant analysis (PLS-DA) models correctly differentiated between authentic (89–100%) and adulterated (90–100%) samples, while partial least-squares regression (PLSR) quantitative models showed poor performance for predicting total offal ( $R^2_{\text{cv}}=0.27\text{--}0.52$ ) and acceptable performance for predicting added fat ( $R^2_{\text{cv}}=0.71\text{--}0.85$ ).

### Other frozen foods

In order to determine the interactions between ice crystals and other food components of in frozen states, Huen et al. (2014) used confocal Raman microscopy to detect frozen bread dough and indicated that this nondestructive method had reliable identification and imaging ability for ice, starch, and gluten, but had low reliability in identifying liquid water and yeast. More importantly, it was shown that the structure of ice crystals appeared as a continuous crystals network rather than as isolated crystals, this new finding may be vital to understand the interactions between ice and gluten because gluten also has a network structure. This means that in the frozen state, the ice crystal network and the gluten network coexist and are embedded in each other.

On the other hand, Camorani et al. (2015) applied Raman spectroscopy to evaluate changes in carotenoid patterns after thermal treatment of frozen carrots and showed that steaming caused a decrease in carotenoid concentration while boiling and microwaving increased carotenoid concentrations. Besides, the trends of Raman spectral parameters exhibited a good statistical correlation with results from conventional techniques, especially high-performance liquid chromatography and colourimetry.

### Limitations and future trends

Other spectroscopic techniques including impedance, fluorescence and near-infrared spectroscopies have been widely used for evaluating the quality of frozen foods. Impedance spectroscopy is extensively applied as an analytical method for determining meat freshness, especially to evaluate structural damages in biological tissues (Egeland et al. 2019; Fuentes et al. 2013). However, this technique cannot provide information about protein secondary structural changes and local environment alterations, structural changes of lipid, and structural alterations of water. Fluorescence spectroscopy is a fundamental analytical technique that can be exploited to study the molecular structure and function (Hassoun et al. 2019; Karoui and Blecker 2011). Karoui and Blecker (2011) summarized the applications of fluorescence spectroscopy for quality determination of animal and vegetable products and showed that fluorescence spectroscopy had the ability to determine function, composition, and nutrition of foods without the employment of chemical reagents, however, fluorescence spectroscopy is unable to obtain detailed information about the secondary structures of protein and is unsuitable for direct detection of samples



in solid-state. Near-infrared spectroscopy is another type of vibrational spectroscopy and has been applied to evaluate meat freshness, predict meat shelf-life, assess meat adulteration, investigate the alterations of lipid, monitor oxidative damage of meat, and identify the quality of fruits during freezing and thawing (Cheng et al. 2018; López-Maestresalas et al. 2019; Tenyang et al. 2019). However, near-infrared spectroscopy can only acquire information about the secondary structures of protein, and the interference from water is strong (Wang et al. 2017). By contrast, Raman spectroscopy can overcome most of the above-mentioned weaknesses and be exploited for aqueous solutions and solid samples, providing information about the molecular vibration related to the structures of protein, lipid, and water.

However, certain limitations are associated with Raman spectroscopy as compared with other spectroscopic techniques. For instance, Fan and Zhang (2019) summarized the applications of NMR for analysis of food compositions, quality discrimination, classification of food, and assessment of food properties relating to physical, chemical, and structure. NMR can be used to measure water distribution and water content in foods, which can indirectly reflect food quality (Ezeanaka, Nsor-Atindana, and Zhang 2019). In NMR, lower (transverse relaxation time) T2 values indicate less mobile water with lower mobility, whereas higher T2 values indicate more mobile water molecules (Cheng et al. 2019), while for Raman spectroscopy, the recognition and investigation of O–H band of liquid water are controversial as discussed previously. Therefore, for further widespread uses in the frozen food industry, these limitations should be overcome in future studies.

- One of the difficulties that interfere with the monitoring of frozen foods is the overlapping of Raman signals. A part of the overlapping Raman signals come from the intrinsic fluorescence characteristic of targeted analytes, and Raman signal intensity is much lower than the fluorescence scattering light. Therefore, the presence of fluorescence signals causes the overlapping of Raman signals, complicating more the recognition of Raman signals. Given this, physical/chemical processing approaches such as light bleaching and surface-enhanced Raman spectroscopy (SERS) have been established and successfully used to remove the fluorescence signals (Fu et al. 2019; Li and Larkin 2020; Yao et al. 2019; Zhai et al. 2015). Besides, multiple data processing techniques such as artificial neural network and chemometric methods also behave satisfactorily in removing fluorescence interferences (He et al. 2019). However, the elimination of fluorescent effects may alter with analyzed samples used. Thus, it is necessary to develop more reliable and efficient fluorescent removal methods in further studies. Another part of the overlapping Raman signals is from other non-targeted analytes. To solve the problems, methods for enhancing the Raman signals like spectral resonance (Jin et al. 2016) and SERS (Yaseen et al. 2019b; Yaseen et al. 2019c) could be a solution to reduce the overlapping signals.

- Noninvasive inspection is an important factor for choosing Raman spectroscopy. However, the complex pretreatment procedures required for preparing the tested samples are essentially invasive, which are unsuitable for online monitoring of frozen foods. Moreover, lengthy laser radiation can produce heat, which may change the conformation of the tested samples and generate measurement errors (Wang et al. 2017). Regarding this, SORS and confocal Raman microscopy are expected to maximally overcome the issues, due to their merits of sub-surface detection and simple pretreatments (Ostovar Pour et al. 2019). Besides, future research and development in light sources can reduce the thermal effect generated by the laser.
- Although Raman spectroscopy has been widely used to determine food quality attributes and discriminate different food materials, there often occur misclassification and quantification errors when studying complex food matrices. One potential solution to minimize sample misclassification is to combine Raman spectroscopy with multi-spectroscopic methods like NIR and mid-infrared because they are complementary techniques that can provide spectral information based on the structure of molecules. Another possible strategy to reduce quantification errors is to develop more effective chemometric multivariate techniques.
- Complex food substances cause difficulties in establishing databases. Therefore, no database related to Raman spectroscopy is available in terms of food analysis. Although Table 2 lists some useful information about Raman bands obtained in food analyses, which should be useful and beneficial for researchers in this area, it is still necessary to conduct more systematic experiments to gather more data and standardize Raman database for further applications in the frozen food industry.
- Raman systems are expensive. The high-cost hinders wide applications of this novel technique for routine detection for the industry. With the development of light source, detector, and computer science, portable and handheld Raman spectroscopy with high-performance and low-cost would become a new trend for the on-line detection of frozen foods.

## Conclusions

Most food products with high moisture contents are highly perishable and require appropriate preservation and effective quality assessment methods. In the current review, the fundamentals, types, applications and possible future trends of Raman spectroscopy in detecting the structure and quality of frozen foods are presented. As an effective analytical technique, Raman spectroscopy can obtain detailed information about structural alterations of frozen foods based on the inelastic scattering of laser light on molecules or molecular groups. Among various Raman spectroscopic techniques, dispersive, Fourier transform, spatially offset, micro and confocal Raman spectroscopies are most commonly used in assessing frozen food quality. In the review, up-to-date

information concerning Raman spectroscopy in evaluating the structural alterations of proteins, lipids, water and other components is provided, with a systematic discussion of the latest structural information of water for the first time, and recent applications covered in using Raman spectroscopic techniques include detecting frozen aquatic products, meat and meat products, and others such as frozen dough. Future trends of developing Raman spectroscopy for detecting frozen foods should focus on reducing overlapping signals, achieving real noninvasive detection, eliminating misclassification and quantification errors, establishing standardized Raman database, and controlling cost.

## Disclosure statement

No potential conflict of interest was reported by the authors.

## Funding

The authors are grateful to the Key R&D Program of Ningxia Hui Autonomous Region (2018BCF01001)/for its support. This research was also supported by the National Key R&D Program of China (2017YFD0400404), the Fundamental Research Funds for the Central Universities (D2190450), the Contemporary International Collaborative Research Centre of Guangdong Province on Food Innovative Processing and Intelligent Control (2019A050519001) and the Common Technical Innovation Team of Guangdong Province on Preservation and Logistics of Agricultural Products (2019KJ145, 2020KJ145).

## References

- Afseth, N. K., M. Bloomfield, J. P. Wold, and P. Matousek. 2014. A novel approach for subsurface through-skin analysis of salmon using spatially offset Raman spectroscopy (SORS). *Applied Spectroscopy* 68 (2):255–62. doi: [10.1366/13-07215](#).
- Badii, F., and N. K. Howell. 2002. Effect of antioxidants, citrate, and cryoprotectants on protein denaturation and texture of frozen cod (*Gadus morhua*). *Journal of Agricultural and Food Chemistry* 50 (7): 2053–61. doi: [10.1021/jf010824f](#).
- Badii, F., and N. K. Howell. 2003. Elucidation of the effect of formaldehyde and lipids on frozen stored cod collagen by FT-Raman spectroscopy and differential scanning calorimetry. *Journal of Agricultural and Food Chemistry* 51 (5):1440–6. doi: [10.1021/jf020492u](#).
- Berhe, D. T., C. E. Eskildsen, R. Lametsch, M. S. Hviid, F. van den Berg, and S. B. Engelsen. 2016. Prediction of total fatty acid parameters and individual fatty acids in pork backfat using Raman spectroscopy and chemometrics: Understanding the cage of covariance between highly correlated fat parameters. *Meat Science* 111:18–26.
- Boireau-Adamezyk, E., A. Baillet-Guffroy, and G. N. Stamatas. 2014. Mobility of water molecules in the stratum corneum: Effects of age and chronic exposure to the environment. *The Journal of Investigative Dermatology* 134 (7):2046–9. doi: [10.1038/jid.2014.96](#).
- Butler, H. J., L. Ashton, B. Bird, G. Cinque, K. Curtis, J. Dorney, K. Esmonde-White, N. J. Fullwood, B. Gardner, P. L. Martin-Hirsch, et al. 2016. Using Raman spectroscopy to characterize biological materials. *Nature Protocols* 11 (4):664–87. doi: [10.1038/nprot.2016.036](#).
- Coulomb, D. 2008. Refrigeration and cold chain serving the global food industry and creating a better future: Two key IIR challenges for improved health and environment. *Trends in Food Science & Technology* 19 (8):413–7.
- Cai, L., L. Nian, G. Zhao, Y. Zhang, L. Sha, and J. Li. 2019. Effect of herring antifreeze protein combined with chitosan magnetic nanoparticles on quality attributes in red sea bream (*Pagrosomus major*). *Food and Bioprocess Technology* 12 (3):409–21. doi: [10.1007/s11947-018-2220-4](#).
- Camorani, P., E. Chiavaro, L. Cristofolini, M. Paciulli, M. Zaupe, A. Visconti, V. Fogliano, and N. Pellegrini. 2015. Raman spectroscopy application in frozen carrot cooked in different ways and the relationship with carotenoids. *Journal of the Science of Food and Agriculture* 95 (11):2185–91. doi: [10.1002/jsfa.7009](#).
- Cao, M., J. Wang, A. Cao, D. Shiuan, R. Guan, L. Cai, and Y. Wang. 2018. The impact of recrystallisation on the freeze-thaw cycles of red seabream (*Pagrus major*) fillets. *International Journal of Food Science & Technology* 54 (5):1642–50.
- Careche, M., A. Herrero, and P. Carmona. 2002. Raman analysis of white spots appearing in the shell of argentine red shrimp (*Pleoticus muelleri*) during frozen storage. *Food Chemistry and Toxicology* 67 (8):2892–5.
- Carey, D. M., and G. M. Korenowski. 1998. Measurement of the Raman spectrum of liquid water. *The Journal of Chemical Physics* 108 (7):2669–75. doi: [10.1063/1.475659](#).
- Chao, K., S. Dhakal, J. Qin, M. Kim, and Y. Peng. 2018. A 1064 nm dispersive Raman spectral imaging system for food safety and quality evaluation. *Applied Sciences* 8 (3):431–48. doi: [10.3390/app8030431](#).
- Chen, Q., Y. Xie, J. Xi, Y. Guo, H. Qian, Y. Cheng, Y. Chen, and W. Yao. 2018. Characterization of lipid oxidation process of beef during repeated freeze-thaw by electron spin resonance technology and Raman spectroscopy. *Food Chemistry* 243:58–64. doi: [10.1016/j.foodchem.2017.09.115](#).
- Chen, Q., Y. Zhang, Y. Guo, Y. Cheng, H. Qian, W. Yao, Y. Xie, and Y. Ozaki. 2020. Non-destructive prediction of texture of frozen/thaw raw beef by Raman spectroscopy. *Journal of Food Engineering* 266: 109693. doi: [10.1016/j.jfoodeng.2019.109693](#).
- Cheng, J. H., B. Nicolai, and D.-W. Sun. 2017. Hyperspectral imaging with multivariate analysis for technological parameters prediction and classification of muscle foods: A review. *Meat Science* 123: 182–91.
- Cheng, S., X. Wang, R. Li, H. Yang, H. Wang, H. Wang, and M. Tan. 2019. Influence of multiple freeze-thaw cycles on quality characteristics of beef semimembranous muscle: With emphasis on water status and distribution by LF-NMR and MRI. *Meat Science* 147:44–52. doi: [10.1016/j.meatsci.2018.08.020](#).
- Cheng, W., D.-W. Sun, H. Pu, and Q. Wei. 2018. Heterospectral two-dimensional correlation analysis with near-infrared hyperspectral imaging for monitoring oxidative damage of pork myofibrils during frozen storage. *Food Chemistry* 248:119–27.
- Dou, Z., L. Wang, J. Hu, W. Fang, C. Sun, and Z. Men. 2020. Hydrogen bonding effect on Raman modes of Formic acid-water binary solutions. *Journal of Molecular Liquids* 313:113595. doi: [10.1016/j.molliq.2020.113595](#).
- Dong, J., X. Li, L. Zhao, H. Xiao, F. Wang, X. Guo, and Y. Zhang. 2007. Raman observation of the interactions between  $\text{NH}_4^+$ ,  $\text{SO}_4^{2-}$ , and  $\text{H}_2\text{O}$  in supersaturated  $(\text{NH}_4)_2\text{SO}_4$  droplets. *The Journal of Physical Chemistry B* 111 (42):12170–6. doi: [10.1021/jp072772o](#).
- Đuričković, I., R. Claverie, P. Bourson, M. Marchetti, J.-M. Chassot, and M. D. Fontana. 2011. Water-ice phase transition probed by Raman spectroscopy. *Journal of Raman Spectroscopy* 42 (6):1408–12. doi: [10.1002/jrs.2841](#).
- Egelandsdal, B., S. M. Abie, S. Bjarnadottir, H. Zhu, H. Kolstad, F. Bjerke, O. G. Martinsen, A. Mason, and D. Munch. 2019. Detectability of the degree of freeze damage in meat depends on analytic-tool selection. *Meat Science* 152:8–19. doi: [10.1016/j.meatsci.2019.02.002](#).
- Ember, K. J. I., M. A. Hoeve, S. L. McAughtrie, M. S. Bergholt, B. J. Dwyer, M. M. Stevens, K. Faulds, S. J. Forbes, and C. J. Campbell. 2017. Raman spectroscopy and regenerative medicine: A review. *NPJ Regenerative Medicine* 2:12. doi: [10.1038/s41536-017-0014-3](#).
- Esmonde-White, K. A., M. Cuellar, C. Uerpmann, B. Lenain, and I. R. Lewis. 2017. Raman spectroscopy as a process analytical technology

- for pharmaceutical manufacturing and bioprocessing. *Anal Bioanal Chem* 409 (3):637–49. doi: [10.1007/s00216-016-9824-1](https://doi.org/10.1007/s00216-016-9824-1).
- Ewen, S., and D. Geoffrey. 2019. *Modern Raman Spectroscopy: A practical approach* (2nd ed.). UK: Wiley Blackwell Press, John Wiley & Sons.
- Ezeanaka, M. C., J. Nsor-Atindana, and M. Zhang. 2019. Online low-field nuclear magnetic resonance (LF-NMR) and magnetic resonance imaging (MRI) for food quality optimization in food processing. *Food and Bioprocess Technology* 12 (9):1435–51. doi: [10.1007/s11947-019-02296-w](https://doi.org/10.1007/s11947-019-02296-w).
- Fan, K., and M. Zhang. 2019. Recent developments in the food quality detected by non-invasive nuclear magnetic resonance technology. *Critical Reviews in Food Science and Nutrition* 59 (14):2202–13. doi: [10.1080/10408398.2018.1441124](https://doi.org/10.1080/10408398.2018.1441124).
- Fowler, S. M., H. Schmidt, R. van de Ven, P. Wynn, and D. L. Hopkins. 2015. Predicting meat quality traits of ovine m. semimembranosus, both fresh and following freezing and thawing, using a hand held Raman spectroscopic device. *Meat Science* 108:138–44.
- Fu, G., D.-W. Sun, H. Pu, and Q. Wei. 2019. Fabrication of gold nanorods for SERS detection of thiabendazole in apple. *Talanta* 195: 841–9. doi: [10.1016/j.talanta.2018.11.114](https://doi.org/10.1016/j.talanta.2018.11.114). 30625626
- Fuentes, A., R. Masot, I. Fernández-Segovia, M. Ruiz-Rico, M. Alcáñiz, and J. M. Barat. 2013. Differentiation between fresh and frozen-thawed sea bream (*Sparus aurata*) using impedance spectroscopy techniques. *Innovative Food Science & Emerging Technologies* 19: 210–7.
- Gao, W., Y. Huang, X. A. Zeng, and M. A. Brennan. 2019. Effect of soluble soybean polysaccharides on freeze-denaturation and structure of myofibrillar protein of bighead carp surimi with liquid nitrogen freezing. *International Journal of Biological Macromolecules* 135: 839–44. doi: [10.1016/j.ijbiomac.2019.05.186](https://doi.org/10.1016/j.ijbiomac.2019.05.186).
- Gomes da Costa, S., A. Richter, U. Schmidt, S. Breuninger, and O. Hollricher. 2019. Confocal Raman microscopy in life sciences. *Morphologie: Bulletin de L'Association Des Anatomistes* 103 (341): 11–6. doi: [10.1016/j.morpho.2018.12.003](https://doi.org/10.1016/j.morpho.2018.12.003).
- Hassoun, A., A. Sahar, L. Lakhal, and A. Ait-Kaddour. 2019. Fluorescence spectroscopy as a rapid and non-destructive method for monitoring quality and authenticity of fish and meat products: Impact of different preservation conditions. *LWT - Food Science and Technology* 103:279–92. doi: [10.1016/j.lwt.2019.01.021](https://doi.org/10.1016/j.lwt.2019.01.021).
- He, H., D.-W. Sun, H. Pu, and L. Huang. 2020. Corrigendum to "Bridging Fe<sub>3</sub>O<sub>4</sub>@Au nanoflowers and Au@Ag nanospheres with aptamer for ultrasensitive SERS detection of aflatoxin B1" [Food Chem. 324 (2020) 126832]. *Food Chemistry* 332:127443 doi: [10.1016/j.foodchem.2020.127443](https://doi.org/10.1016/j.foodchem.2020.127443). PMC: 32622187
- He, H., D.-W. Sun, H. Pu, L. Chen, and L. Lin. 2019. Applications of Raman spectroscopic techniques for quality and safety evaluation of milk: A review of recent developments. *Critical Reviews in Food Science and Nutrition* 59 (5):770–93. doi: [10.1080/10408398.2018.1528436](https://doi.org/10.1080/10408398.2018.1528436).
- Herrero, A. M. 2008a. Raman spectroscopy a promising technique for quality assessment of meat and fish: A review. *Food Chemistry* 107 (4):1642–51. doi: [10.1016/j.foodchem.2007.10.014](https://doi.org/10.1016/j.foodchem.2007.10.014).
- Herrero, A. M. 2008b. Raman spectroscopy for monitoring protein structure in muscle food systems. *Critical Reviews in Food Science and Nutrition* 48 (6):512–23.
- Herrero, A. M., P. Carmona, and M. Careche. 2004. Raman spectroscopic study of structural changes in hake (*Merluccius merluccius* L.) muscle proteins during frozen storage. *Journal of Agricultural and Food Chemistry* 52 (8):2147–53. doi: [10.1021/jf034301e](https://doi.org/10.1021/jf034301e).
- Hu, B., D.-W. Sun, H. Pu, and Q. Wei. 2020a. Rapid nondestructive detection of mixed pesticides residues on fruit surface using SERS combined with self-modeling mixture analysis method. *Talanta* 217: 120998 doi: [10.1016/j.talanta.2020.120998](https://doi.org/10.1016/j.talanta.2020.120998). PMC: 32498854
- Hu, B., D.-W. Sun, H. Pu, and Q. Wei. 2020b. A dynamically optical and highly stable pNIPAM @ Au NRs nanohybrid substrate for sensitive SERS detection of malachite green in fish fillet. *Talanta* 218: 121188 doi: [10.1016/j.talanta.2020.121188](https://doi.org/10.1016/j.talanta.2020.121188). PMC: 32797928
- Hubbard, T. J. E., A. Shore, and N. Stone. 2019. Raman spectroscopy for rapid intra-operative margin analysis of surgically excised tumour specimens. *The Analyst* 144 (22):6479–96. doi: [10.1039/c9an01163c](https://doi.org/10.1039/c9an01163c).
- Huen, J., C. Weikusat, M. Bayer-Giraldi, I. Weikusat, L. Ringer, and K. Lösche. 2014. Confocal Raman microscopy of frozen bread dough. *Journal of Cereal Science* 60 (3):555–60. doi: [10.1016/j.jcs.2014.07.012](https://doi.org/10.1016/j.jcs.2014.07.012).
- Hussain, A., D.-W. Sun, and H. Pu. 2019. SERS detection of urea and ammonium sulfate adulterants in milk with coffee ring effect. *Food Additives & Contaminants. Part A, Chemistry, Analysis, Control, Exposure & Risk Assessment* 36 (6):851–62. doi: [10.1080/19440049.2019.1591643](https://doi.org/10.1080/19440049.2019.1591643). 31034331
- Hussain, A., D.-W. Sun, and H. Pu. 2020a. Bimetallic core shelled nanoparticles (Au@AgNPs) for rapid detection of thiram and dicyandiamide contaminants in liquid milk using SERS. *Food Chemistry* 317:126429 doi: [10.1016/j.foodchem.2020.126429](https://doi.org/10.1016/j.foodchem.2020.126429). PMC: 32109658
- Hussain, A., H. Pu, and D.-W. Sun. 2020b. SERS detection of sodium thiocyanate and benzoic acid preservatives in liquid milk using cysteamine functionalized core-shelled nanoparticles. *Spectrochimica Acta. Part A, Molecular and Biomolecular Spectroscopy* 229:117994 doi: [10.1016/j.saa.2019.117994](https://doi.org/10.1016/j.saa.2019.117994). PMC: 31951941
- Hussain, A., H. Pu, and D.-W. Sun. 2020c. Cysteamine modified core-shell nanoparticles for rapid assessment of oxamyl and thiacloprid pesticides in milk using SERS. *Journal of Food Measurement and Characterization* 14 (4):2021–9. doi: [10.1007/s11694-020-00448-7](https://doi.org/10.1007/s11694-020-00448-7).
- Hussain, N., H. Pu, A. Hussain, and D.-W. Sun. 2020. Rapid detection of ziram residues in apple and pear fruits by SERS based on octanethiol functionalized bimetallic core-shell nanoparticles. *Spectrochimica Acta. Part A, Molecular and Biomolecular Spectroscopy* 236:118357 doi: [10.1016/j.saa.2020.118357](https://doi.org/10.1016/j.saa.2020.118357). PMC: 32375074
- Jayan, H., H. Pu, and D.-W. Sun. 2020. Recent development in rapid detection techniques for microorganism activities in food matrices using bio-recognition: A review. *Trends in Food Science & Technology* 95:233–46. doi: [10.1016/j.tifs.2019.11.007](https://doi.org/10.1016/j.tifs.2019.11.007).
- Jermyn, M., J. Desroches, K. Aubertin, K. St-Arnaud, W. J. Madore, E. De Montigny, M. C. Guioit, D. Trudel, B. C. Wilson, K. Petrecca, et al. 2016. A review of Raman spectroscopy advances with an emphasis on clinical translation challenges in oncology. *Physics in Medicine and Biology* 61 (23):R370–R400. doi: [10.1088/0031-9155/61/23/R370](https://doi.org/10.1088/0031-9155/61/23/R370).
- Jin, H., Q. Lu, X. Chen, H. Ding, H. Gao, and S. Jin. 2016. The use of Raman spectroscopy in food processes: A review. *Applied Spectroscopy Reviews* 51 (1):12–22. doi: [10.1080/05704928.2015.1087404](https://doi.org/10.1080/05704928.2015.1087404).
- Kang, T., Y. You, and S. Jun. 2020. Supercooling preservation technology in food and biological samples: A review focused on electric and magnetic field applications. *Food Science and Biotechnology* 29 (3):303–21. doi: [10.1007/s10068-020-00750-6](https://doi.org/10.1007/s10068-020-00750-6).
- Kang, Z. L., P. Wang, X. L. Xu, C. Z. Zhu, K. Li, and G. H. Zhou. 2014. Effect of beating processing, as a means of reducing salt content in frankfurters: A physico-chemical and Raman spectroscopic study. *Meat Science* 98 (2):171–7. doi: [10.1016/j.meatsci.2014.05.025](https://doi.org/10.1016/j.meatsci.2014.05.025).
- Karoui, R., and C. Blecker. 2011. Fluorescence spectroscopy measurement for quality assessment of food systems—A review. *Food and Bioprocess Technology* 4 (3):364–86. doi: [10.1007/s11947-010-0370-0](https://doi.org/10.1007/s11947-010-0370-0).
- Krimm, S., and J. Bandekar. 1986. Vibrational spectroscopy and conformation of peptides, polypeptides, and proteins. *Advances in Protein Chemistry* 38:181–364. doi: [10.1016/s0065-3233\(08\)60528-8](https://doi.org/10.1016/s0065-3233(08)60528-8).
- Leelapongwattana, K., S. Benjakul, W. Visessanguan, and N. K. Howell. 2008. Raman spectroscopic analysis and rheological measurements on natural actomyosin from haddock (*Melanogrammus aeglefinus*) during refrigerated (4 °C) and frozen (−10 °C) storage in the presence of trimethylamine-N-oxide demethylase from kidney of lizard-fish (*Saurida tumbil*). *Food Chemistry* 106 (3):1253–63. doi: [10.1016/j.foodchem.2007.06.061](https://doi.org/10.1016/j.foodchem.2007.06.061).
- Li-Chan, E. C. Y. 1996. The applications of Raman spectroscopy in food science. *Trends in Food Science & Technology* 7 (11):361–70.



- Li, D., Z. Zhu, and D.-W. Sun. 2018a. Effects of freezing on cell structure of fresh cellular food materials: A review. *Trends in Food Science & Technology* 75:46–55. doi: [10.1016/j.tifs.2018.02.019](https://doi.org/10.1016/j.tifs.2018.02.019).
- Li, D., Z. Zhu, and D.-W. Sun. 2020b. Visualization of the in situ distribution of contents and hydrogen bonding states of cellular level water in apple tissues by confocal Raman microscopy. *The Analyst* 145 (3):897–907.
- Li, B., and P. J. Larkin. 2020. Chemical bleaching to minimize Fluorescence interference in Raman spectroscopic measurements for sulfonated polystyrene solutions. *Applied Spectroscopy* 74 (7):741–50.
- Li, Y. S., and J. S. Church. 2014. Raman spectroscopy in the analysis of food and pharmaceutical nanomaterials. *Journal of Food and Drug Analysis* 22 (1):29–48. doi: [10.1016/j.jfda.2014.01.003](https://doi.org/10.1016/j.jfda.2014.01.003).
- López-Maestresalas, A., K. Insausti, C. Jarén, C. Pérez-Roncal, O. Urrutia, M. J. Beriain, and S. Arazuri. 2019. Detection of minced lamb and beef fraud using NIR spectroscopy. *Food Control* 98: 465–73. doi: [10.1016/j.foodcont.2018.12.003](https://doi.org/10.1016/j.foodcont.2018.12.003).
- Ma, C., and D. L. Phillips. 2002. FT-Raman spectroscopy and its applications in cereal science. *Cereal Chemistry Journal* 79 (2):171–7. doi: [10.1094/CCHEM.2002.79.2.171](https://doi.org/10.1094/CCHEM.2002.79.2.171).
- Ma, J., H. Pu, D.-W. Sun, W. Gao, J.-H. Qu, and K.-Y. Ma. 2015. Application of Vis-NIR hyperspectral imaging in classification between fresh and frozen-thawed pork Longissimus Dorsi muscles. *International Journal of Refrigeration* 50:10–8. doi: [10.1016/j.ijrefrig.2014.10.024](https://doi.org/10.1016/j.ijrefrig.2014.10.024).
- Matousek, P. 2018. Spatially offset Raman spectroscopy for non-invasive analysis of turbid samples. *TrAC Trends in Analytical Chemistry* 103:209–14. doi: [10.1016/j.trac.2018.04.002](https://doi.org/10.1016/j.trac.2018.04.002).
- Matousek, P., and N. Stone. 2016. Development of deep subsurface Raman spectroscopy for medical diagnosis and disease monitoring. *Chemical Society Reviews* 45 (7):1794–802. doi: [10.1039/c5cs00466g](https://doi.org/10.1039/c5cs00466g).
- Muik, B., B. Lendl, A. Molina-Díaz, and M. J. Ayora-Canada. 2005. Direct monitoring of lipid oxidation in edible oils by Fourier transform Raman spectroscopy. *Chemistry and Physics of Lipids* 134 (2): 173–82. doi: [10.1016/j.chemphyslip.2005.01.003](https://doi.org/10.1016/j.chemphyslip.2005.01.003).
- Nian, L., A. Cao, L. Cai, H. Ji, and S. Liu. 2019. Effect of vacuum impregnation of red sea bream (*Pagrosomus major*) with herring AFP combined with CS@Fe<sub>3</sub>O<sub>4</sub> nanoparticles during freeze-thaw cycles. *Food Chemistry* 291:139–48. doi: [10.1016/j.foodchem.2019.04.017](https://doi.org/10.1016/j.foodchem.2019.04.017).
- Nian, Y., M. Zhao, C. P. O'Donnell, G. Downey, J. P. Kerry, and P. Allen. 2017. Assessment of physico-chemical traits related to eating quality of young dairy bull beef at different ageing times using Raman spectroscopy and chemometrics. *Food Research International (Ottawa, Ont.)* 99 (Pt 1):778–89.
- Ostovar Pour, S., S. M. Fowler, D. L. Hopkins, P. J. Torley, H. Gill, and E. W. Blanch. 2019. Investigation of chemical composition of meat using spatially off-set Raman spectroscopy. *The Analyst* 144 (8):2618–27. doi: [10.1039/c8an01958d](https://doi.org/10.1039/c8an01958d).
- Qu, J.-H., J.-H. Cheng, D.-W. Sun, H. Pu, Q.-J. Wang, and J. Ma. 2015a. Discrimination of shelled shrimp (*Metapenaeus ensis*) among fresh, frozen-thawed and cold-stored by hyperspectral imaging technique. *LWT - Food Science and Technology* 62 (1):202–9. doi: [10.1016/j.lwt.2015.01.018](https://doi.org/10.1016/j.lwt.2015.01.018).
- Qu, J. H., D. Liu, J. H. Cheng, D.-W. Sun, J. Ma, H. Pu, and X. A. Zeng. 2015b. Applications of near-infrared spectroscopy in food safety evaluation and control: A review of recent research advances. *Critical Reviews in Food Science and Nutrition* 55 (13):1939–54.
- Ratcliffe, C. L., and D. E. Irish. 1982. Vibrational spectral studies of solutions at elevated temperatures and pressures. 5. Raman studies of liquid water up to 300.degree.C. *Journal of Solution Chemistry* 17 (9):805–24.
- Rygula, A., K. Majzner, K. M. Marzec, A. Kaczor, M. Pilarczyk, and M. Baranska. 2013. Raman spectroscopy of proteins: A review. *Journal of Raman Spectroscopy* 44 (8):1061–76. doi: [10.1002/jrs.4335](https://doi.org/10.1002/jrs.4335).
- Sanchez-Alonso, I., P. Carmona, and M. Careche. 2012. Vibrational spectroscopic analysis of hake (*Merluccius merluccius* L.) lipids during frozen storage. *Food Chemistry* 132 (1):160–7.
- Sánchez-González, I., P. Carmona, P. Moreno, J. Borderías, I. Sánchez-Alonso, A. Rodríguez-Casado, and M. Careche. 2008. Protein and water structural changes in fish surimi during gelation as revealed by isotopic H/D exchange and Raman spectroscopy. *Food Chemistry* 106 (1):56–64. doi: [10.1016/j.foodchem.2007.05.067](https://doi.org/10.1016/j.foodchem.2007.05.067).
- Sarkardei, S., and N. K. Howell. 2007. The effects of freeze-drying and storage on the FT-Raman spectra of Atlantic mackerel (*Scomber scombrus*) and horse mackerel (*Trachurus trachurus*). *Food Chemistry* 103 (1):62–70. doi: [10.1016/j.foodchem.2006.06.065](https://doi.org/10.1016/j.foodchem.2006.06.065).
- Schmidt, H., R. Scheier, and D. L. Hopkins. 2013. Preliminary investigation on the relationship of Raman spectra of sheep meat with shear force and cooking loss. *Meat Science* 93 (1):138–43. doi: [10.1016/j.meatsci.2012.08.019](https://doi.org/10.1016/j.meatsci.2012.08.019).
- Schulz, H., M. Baranska, and R. Baranski. 2005. Potential of NIR-FT-Raman spectroscopy in natural carotenoid analysis. *Biopolymers* 77 (4):212–21. doi: [10.1002/bip.20215](https://doi.org/10.1002/bip.20215).
- Sun, Q. 2009. The Raman OH stretching bands of liquid water. *Vibrational Spectroscopy* 51 (2):213–7. doi: [10.1016/j.vibspec.2009.05.002](https://doi.org/10.1016/j.vibspec.2009.05.002).
- Sun, W., Q. Zhao, M. Zhao, B. Yang, C. Cui, and J. Ren. 2011. Structural evaluation of myofibrillar proteins during processing of Cantonese sausage by Raman spectroscopy. *Journal of Agricultural and Food Chemistry* 59 (20):11070–7. doi: [10.1021/jf202560s](https://doi.org/10.1021/jf202560s).
- Tao, F., and M. Ngadi. 2018. Recent advances in rapid and nondestructive determination of fat content and fatty acids composition of muscle foods. *Critical Reviews in Food Science and Nutrition* 58 (9): 1565–93. doi: [10.1080/10408398.2016.1261332](https://doi.org/10.1080/10408398.2016.1261332).
- Teixeira Dos Santos, C. A., R. Pascoa, M. C. Sarraguça, P. Porto, A. L. Cerdeira, J. M. Gonzalez-Saiz, C. Pizarro, and J. A. Lopes. 2017. Merging vibrational spectroscopic data for wine classification according to the geographic origin. *Food Research International (Ottawa, Ont.)* 102:504–10. doi: [10.1016/j.foodres.2017.09.018](https://doi.org/10.1016/j.foodres.2017.09.018).
- Tenyang, N., B. Tiencheu, F. Tonfack Djikeng, A. T. Morfor, and H. M. Womeni. 2019. Alteration of the lipid of red carp (*Cyprinus carpio*) during frozen storage. *Food Science & Nutrition* 7 (4): 1371–8. doi: [10.1002/fsn3.971](https://doi.org/10.1002/fsn3.971).
- Thygesen, L. G., M. M. Løkke, E. Micklander, and S. B. Engelsen. 2003. Vibrational microspectroscopy of food. Raman vs. FT-IR. *Trends in Food Science & Technology* 14 (1-2):50–7.
- Tian, Y., Z. Chen, Z. Zhu, and D.-W. Sun. 2020a. Effects of tissue predegassing followed by ultrasound-assisted freezing on freezing efficiency and quality attributes of radishes. *Ultrasonics Sonochemistry* 67:105162.
- Tian, Y., D. Li, W. Luo, Z. Zhu, W. Li, Z. Qian, G. Li, and D.-W. Sun. 2020b. Rapid freezing using atomized liquid nitrogen spray followed by frozen storage below glass transition temperature for Cordyceps sinensis preservation: Quality attributes and storage stability. *LWT - Food Science and Technology* 123:109066. doi: [10.1016/j.lwt.2020.109066](https://doi.org/10.1016/j.lwt.2020.109066).
- Tian, Y., P. Zhang, Z. Zhu, and D.-W. Sun. 2020c. Development of a single/dual-frequency orthogonal ultrasound-assisted rapid freezing technique and its effects on quality attributes of frozen potatoes. *Journal of Food Engineering* 286:110112. doi: [10.1016/j.jfoodeng.2020.110112](https://doi.org/10.1016/j.jfoodeng.2020.110112).
- Velioglu, H. M., H. T. Temiz, and I. H. Boyaci. 2015. Differentiation of fresh and frozen-thawed fish samples using Raman spectroscopy coupled with chemometric analysis. *Food Chemistry* 172:283–90.
- Wang, K., D.-W. Sun, H. Pu, Q. Wei, and L. Huang. 2019a. Stable, Flexible, and High-Performance SERS Chip Enabled by a Ternary Film-Packaged Plasmonic Nanoparticle Array. *ACS Applied Materials & Interfaces* 11 (32):29177–86. doi: [10.1021/acsami.9b09746](https://doi.org/10.1021/acsami.9b09746). 31317741
- Wang, K., D.-W. Sun, H. Pu, and Q. Wei. 2019b. Shell thickness-dependent Au@Ag nanoparticles aggregates for high-performance SERS applications. *Talanta* 195:506–15. doi: [10.1016/j.talanta.2018.11.057](https://doi.org/10.1016/j.talanta.2018.11.057). 30625576
- Wang, K., D.-W. Sun, H. Pu, and Q. Wei. 2019c. Surface-enhanced Raman scattering of core-shell Au@Ag nanoparticles aggregates for rapid detection of difenoconazole in grapes. *Talanta* 191:449–56. doi: [10.1016/j.talanta.2018.08.005](https://doi.org/10.1016/j.talanta.2018.08.005).
- Wang, K., D.-W. Sun, H. Pu, and Q. Wei. 2020a. A rapid dual-channel readout approach for sensing carbendazim with 4-

- aminobenzenethiol-functionalized core-shell Au@Ag nanoparticles. *The Analyst* 145 (5):1801–9. doi:[10.1039/c9an02185j](https://doi.org/10.1039/c9an02185j). 31951224
- Wang, K., D.-W. Sun, H. Pu, and Q. Wei. 2020b. Two-dimensional Au@Ag nanodot array for sensing dual-fungicides in fruit juices with surface-enhanced Raman spectroscopy technique. *Food Chemistry* 310:125923. doi:[10.1016/j.foodchem.2019.125923](https://doi.org/10.1016/j.foodchem.2019.125923). PMC: 31837530
- Wang, K., D.-W. Sun, H. Pu, and Q. Wei. 2017. Principles and applications of spectroscopic techniques for evaluating food protein conformational changes: A review. *Trends in Food Science & Technology* 67:207–19.
- Wang, W. T., H. Zhang, Y. Yuan, Y. Guo, and S. X. He. 2018. Research Progress of Raman Spectroscopy in Drug Analysis. *AAPS PharmSciTech* 19 (7):2921–8. doi: [10.1208/s12249-018-1135-8](https://doi.org/10.1208/s12249-018-1135-8).
- Wu, L., H. Pu, L. Huang, and D.-W. Sun. 2020. Plasmonic nanoparticles on metal-organic framework: A versatile SERS platform for adsorptive detection of new coccine and orange II dyes in food. *Food Chemistry* 328:127105. doi:[10.1016/j.foodchem.2020.127105](https://doi.org/10.1016/j.foodchem.2020.127105). PMC: 32464556
- Xie, A., D.-W. Sun, Z. Xu, and Z. Zhu. 2015. Rapid detection of frozen pork quality without thawing by Vis-NIR hyperspectral imaging technique. *Talanta* 139:208–15. doi: [10.1016/j.talanta.2015.02.027](https://doi.org/10.1016/j.talanta.2015.02.027).
- Yang, D., and Y. Ying. 2011. Applications of Raman Spectroscopy in Agricultural Products and Food Analysis: A Review. *Applied Spectroscopy Reviews* 46 (7):539–60. doi: [10.1080/05704928.2011.593216](https://doi.org/10.1080/05704928.2011.593216).
- Yao, Z. X., H. Su, Y. Han, J. G. Xu, X. C. Huang, and X. Xin. 2019. Fluorescence Fading Effect and Raman Spectrum Baseline Interference Cancellation. *Spectroscopy and Spectral Analysis* 39 (7): 2034–9.
- Yaseen, T., H. Pu, and D.-W. Sun. 2019c. Fabrication of silver-coated gold nanoparticles to simultaneously detect multi-class insecticide residues in peach with SERS technique. *Talanta* 196:537–45. doi:[10.1016/j.talanta.2018.12.030](https://doi.org/10.1016/j.talanta.2018.12.030). 30683402
- Yaseen, T., H. Pu, and D.-W. Sun. 2019b. Rapid detection of multiple organophosphorus pesticides (triazophos and parathion-methyl) residues in peach by SERS based on core-shell bimetallic Au@Ag NPs. *Food Additives & Contaminants. Part A, Chemistry, Analysis, Control, Exposure & Risk Assessment* 36 (5):762–78. doi:[10.1080/19440049.2019.1582806](https://doi.org/10.1080/19440049.2019.1582806). 30943113
- Yu, N., B. H. Jo, and D. C. O'Shea. 1973. Laser Raman scattering of cobramine B, a basic protein from cobra venom. *Archives of Biochemistry and Biophysics* 156 (1):71–6. doi: [10.1016/0003-9861\(73\)90342-1](https://doi.org/10.1016/0003-9861(73)90342-1).
- Zhai, C., Y. Peng, Y. Li, and T. Xu. 2015. Nondestructive detection of chlorpyrifos in apples based on surface enhanced raman scattering. *Acta Chimica Sinica* 73 (11):1167–72. doi: [10.6023/A15050326](https://doi.org/10.6023/A15050326).
- Zhan, X., Z. Zhu, and D.-W. Sun. 2019. Effects of pretreatments on quality attributes of long-term deep frozen storage of vegetables: A review. *Critical Reviews in Food Science and Nutrition* 59 (5):743–57. doi: [10.1080/10408398.2018.1496900](https://doi.org/10.1080/10408398.2018.1496900).
- Zhang, T., Z. Li, Y. Wang, Y. Xue, and C. Xue. 2016. Effects of konjac glucomannan on heat-induced changes of physicochemical and structural properties of surimi gels. *Food Research International* 83: 152–61. doi: [10.1016/j.foodres.2016.03.007](https://doi.org/10.1016/j.foodres.2016.03.007).
- Zhang, Y., and P. Ertbjerg. 2019. On the origin of thaw loss: Relationship between freezing rate and protein denaturation. *Food Chemistry* 299:125104. doi: [10.1016/j.foodchem.2019.125104](https://doi.org/10.1016/j.foodchem.2019.125104).
- Zhao, M., G. Downey, and C. P. O'Donnell. 2015. Dispersive Raman spectroscopy and multivariate data analysis to detect offal adulteration of thawed beefburgers. *Journal of Agricultural and Food Chemistry* 63 (5):1433–41. doi: [10.1021/jf5041959](https://doi.org/10.1021/jf5041959).
- Zhou, L., C. Zhang, Z. Qiu, and Y. He. 2020. Information fusion of emerging non-destructive analytical techniques for food quality authentication: A survey. *TrAC Trends in Analytical Chemistry* 127: 115901. doi: [10.1016/j.trac.2020.115901](https://doi.org/10.1016/j.trac.2020.115901).
- Zhou, X., H. Chen, F. Lyu, H. Lin, Q. Zhang, and Y. Ding. 2019. Physicochemical properties and microstructure of fish myofibrillar protein-lipid composite gels: Effects of fat type and concentration. *Food Hydrocolloids* 90:433–42. doi: [10.1016/j.foodhyd.2018.12.032](https://doi.org/10.1016/j.foodhyd.2018.12.032).
- Zhou, X., S. Jiang, D. Zhao, J. Zhang, S. Gu, Z. Pan, and Y. Ding. 2017. Changes in physicochemical properties and protein structure of surimi enhanced with camellia tea oil. *LWT - Food Science and Technology* 84:562–71. doi: [10.1016/j.lwt.2017.03.026](https://doi.org/10.1016/j.lwt.2017.03.026).
- Zhu, Y., Y. Li, C. Wu, F. Teng, B. Qi, X. Zhang, L. Zhou, G. Yu, H. Wang, S. Zhang, et al. 2019. Stability mechanism of two soybean protein-phosphatidylcholine nanoemulsion preparation methods from a structural perspective: A Raman Spectroscopy analysis. *Scientific Reports* 9 (1):6985
- Zhu, Z., P. Zhang, and D.-W. Sun. 2020a. Effects of multi-frequency ultrasound on freezing rates and quality attributes of potatoes. *Ultrasonics Sonochemistry* 60:104733.
- Zhu, Z., Q. Zhou, and D.-W. Sun. 2019b. Measuring and controlling ice crystallization in frozen foods: A review of recent developments. *Trends in Food Science & Technology* 90:13–25. doi: [10.1016/j.tifs.2019.05.012](https://doi.org/10.1016/j.tifs.2019.05.012).